https://doi.org/10.1016/j.rser.2018.03.024

Recent advances in alkali-doped polybenzimidazole membranes for fuel cell applications

Q.X. Wu[a], Z.F. Pan[b] and L. An[b]*

[a] Shenzhen Key Laboratory of New Lithium-ion Batteries and Mesoporous Materials, College of Chemistry and Environmental Engineering, Shenzhen University, Shenzhen 518060, Guangdong, China

[b] Department of Mechanical Engineering, The Hong Kong Polytechnic University, Hung Hom, Kowloon, Hong Kong SAR, China

*Corresponding author.

[b] Email: liang.an@polyu.edu.hk (L. An)

Abstract

Polybenzimidazole (PBI), with a well-known excellent thermal stability, has been recognized as an alternative for anion exchange membrane fuel cells (AEMFC), primarily because it can serve as an ionic conductor after doping with inorganic hydroxides (typically KOH/NaOH) and thus allows fuel cells to be operated at high temperatures (currently as high as 120^{o}C). In addition, alkali-doped PBI membranes also offer many other favored physiochemical properties, such as high ionic conductivity. The objective of this article is to provide a review of recent research on

the alkali-doped PBI membranes and their application in fuel cells, including mechanisms of ion conduction through the alkali-doped PBI membranes, stability of the PBI membranes doped with alkali, strategies aiming at improving the ionic conductivity of the PBI membranes doped with alkali, as well as the performance of alkali-doped PBI membrane based fuel cells. Additionally, future perspectives relating to the development of alkali-doped PBI membranes and their applications in fuel cells are also highlighted.

Keywords: Fuel cells; Anion exchange membrane fuel cells; Polybenzimidazole; Alkali-doped PBI membranes; Physiochemical properties; Single-cell performance

1. Introduction

Anion exchange membrane fuel cells (AEMFC) are generally regarded as an emerging energy conversion technology that has the potential to overcome many obstacles of proton exchange membrane fuel cells (PEMFC) in cost, stability, and durability of materials [1-10]. The typical structure design of AEMFC systems is analogous to that of PEMFCs, where the ion transport pathways are established between the cathode and anode. It is attributed to the dispersed ionomers with a network inside the electrodes, which are interfaced with the membrane [11-16]. Nevertheless, the performance of such a fuel cell system where transporting the hydroxide ions through the membrane purely relies on an AEM and ionomers in the electrodes is not satisfactory, primarily due to the low conductivity of state-of-the-art AEMs and corresponding ionomers [17-21]. In addition, another obstacle limiting the cell power output of AEMFCs is that current AEMs fabricated into fuel cells are not capable to be operated at high temperatures (< 60^{o}C) [22-24]. It has been recently demonstrated that polybenizimidazole (PBI) can withstand the high-temperature operation, and after doping with inorganic acid, the membranes can conduct protons and thus be used in fuel cells [25-37]. Among them, Wainright et al. [31] firstly introduced PBI membranes doped with acid for high-temperature PEMFCs. Similarly, Xing et al. [37] examined alkali-doped PBI membranes for AEMFCs. The highest

conductivity of KOH-doped PBI (9×10^{-2} S cm^{-1} at 25°C) was higher than those of H_2SO_4-doped PBI membrane (5×10^{-2} S cm^{-1} at 25°C) and H_3PO_4-doped PBI membrane (2×10^{-2} S cm^{-1} at 25°C). More impressively, they showed that the hydrogen/oxygen fuel cells with an alkali-doped PBI membrane and a Nafion 117 membrane exhibited the same performance [37].

Since the pioneering work done by Xing et al. [37], extensive attentions haven been paid to the alkali-doped PBI membranes, which become an alternative to the conventional QA-based AEMs in AEMFCs over the past decade [37-43]. As a consequence, great progress has been made in facilitating the large-scale utilization of this membrane in practical applications, but several critical issues are still remaining to be resolved, such as alkali leakage, high fuel permeability, and poor mechanical stability. This review focuses on recent advances and development of alkali-doped PBI membranes for fuel cell applications. In this article, we start with the mechanisms of ion conduction through the alkali-doped PBI membranes and the chemical structure change after doping, followed by the detailed discussion about the stability of the alkali-doped PBI membranes, including thermal stability, mechanical stability, and liquid uptake. Moreover, the strategies to promote the ionic conductivity of the PBI membranes doped with alkali are also summarized and compared. Meanwhile, the effects of the doping time, alkali type and concentration, carbonate presence,

temperature, and soaking time on the ionic conductivity are described and discussed, respectively. Finally, we summarize and discuss the single-cell performance achieved by using the alkali-doped PBI membranes in fuel cells running on various fuels, including hydrogen, methanol, ethanol, and other alcohols.

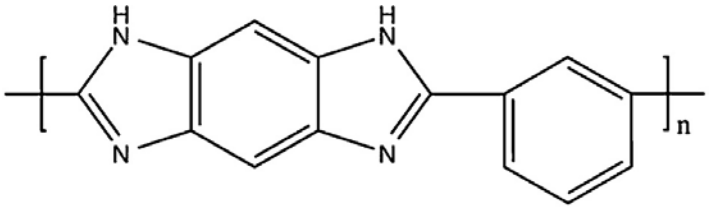

Fig. 1 Chemical structure of the pristine polybenzimidazole membrane [59]. Reproduced with permission from Elsevier.

2. Mechanisms of ion conduction through the alkali-doped polybenzimidazole membrane

The ion exchange membranes used in fuel cells are expected to meet the following requirements: high performance, high durability, but low cost. The function of the ion exchange membranes installed in fuel cells is to separate two electrodes (electron insulator), conduct ions (ion conductor), and be impermeable to fuels (fuel insulator). In AEMFCs, a barrier that limits their performance is that current AEMs fabricated into fuel cells are not capable to be operated at high temperatures (typically < 60^{o}C). It has been recently demonstrated that alkali-doped PBI membranes can offer the good thermal property and high ionic conductivity. For this reason, much attention has been extensively paid to this type of membrane. In fact, the pristine PBI

membrane is primarily an electron and ion insulator (ionic conductivity: 1×10^{-12} S cm^{-1} [44]) and its chemical structure is shown in Fig. 1. Like doping with inorganic acid, adding the pyrrole-type nitrogen (-NH-) and the pyridine-type nitrogen (-N=) in the benzimidazole rings is in favor of absorbing and interacting with the free inorganic base, which is capable of conducting ions [45]. Generally, the pristine PBI membrane is pre-treated to form the ion-conductive membrane by immersing it in an alkaline electrolyte solution (typically NaOH/KOH [37, 38, 45]) or in an alkaline fuel-electrolyte-mixed solution (typically ethanol/methanol + NaOH/KOH [39, 46]), for a certain period of time. Zeng et al. [45] investigated the morphology change of the PBI membrane doped with alkali comparing to the PBI membrane via SEM-EDS. It was shown that the membrane possessed a uniform, dense and smooth structure after doping. In addition, it was also shown that after doping, the potassium and oxygen that were derived from the doped alkali were distributed through the whole membrane uniformly. They further investigated the morphology change during doping via AFM. It was found that the original PBI membrane was hydrophobic as a result of showing a bright field; while, the hydrophilic domains appeared after doping. Also, Hou et al. [39] studied the PBI membranes doped with alkali through the cross-sectional SEM images and its corresponding EDX mappings for elements of K, O, and N. Similarly, it was demonstrated that the elements of K, O, and N were

distributed homogeneously. They explained that the presence of potassium was attributed to the reaction between KOH and -NH- in addition to the free KOH in the matrix, both of which were beneficial to the ion conduction.

In addition, the doping process also changes the chemical structure of the membrane. Zeng et al. [45] investigated the chemical structure change of the membrane doped with alkali comparing to the PBI membrane via FTIR. The results showed that the -NH- stretching vibration (1284 cm^{-1}) was replaced by -NK- deformation (1510 cm^{-1}) and bending vibration (1120 cm^{-1}), indicating that the reaction between cations (K^+) and benzimidazole segments in the PBI skeleton caused partial fracture of the hydrogen bonds. They further confirmed the chemical structure change of the membrane doped with alkali comparing to the PBI membrane via XPS, and found that after doping, the emergence of the potassium peaks indicated the successful formation of the PBI membrane doped with alkali.

Based on the above-mentioned characterizations before and after doping, there are a few mechanisms proposed for formation of the alkali-doped PBI membrane [39, 45, 47]. For example, Hou et al. [39] proposed a doping mechanism for alkali-doped PBI membranes, as shown in Fig. 2a. Firstly, the interaction between K^+ and -NH- in imidazole ring occurred due to neutralization. Secondly, the existence of hydrogen bonding was detected between -N- and OH^- in imidazole ring; meanwhile, K^+ was

133 brought into the polymer to balance OH^-. They also confirmed this result via DFT
134 calculations [47]. Based on the DFT results, they proposed a detailed mechanism, as
135 illustrated in Fig. 2b. (i) -NH- can dissociate into H^+ and -N-; (ii) the dissociated H^+
136 can combine with OH^- to form H_2O; and (iii) K^+ has to combine with -N- to form
137 -NK-. Recently, Zeng et al. [45] also proposed a similar doping mechanism for the
138 PBI membrane immersed in alkaline solutions, as illustrated in Fig. 2c. Firstly, the the
139 pyrrole-type nitrogen (-NH-) in pristine PBI membrane dissociated protons and then
140 the dissociated protons reacted with the hydroxide ions (OH^-). Hence, the first step
141 can be presented by a neutralization reaction. Secondly, the potassium cations (K^+)
142 are functioned in bridging nitrogen atoms that are negatively charged. In addition, the
143 hydrophilic ionic clusters will established to conduct the hydroxide ions by
144 combination between the KOH solution and the PBI matrix, as illustrated in Fig. 2d.
145 With a higher KOH concentration, the hydrophilic ionic clusters will become larger,
146 which is the reason that the conductivity of the PBI membranes doped with alkali
147 increases with higher KOH concentration [45].

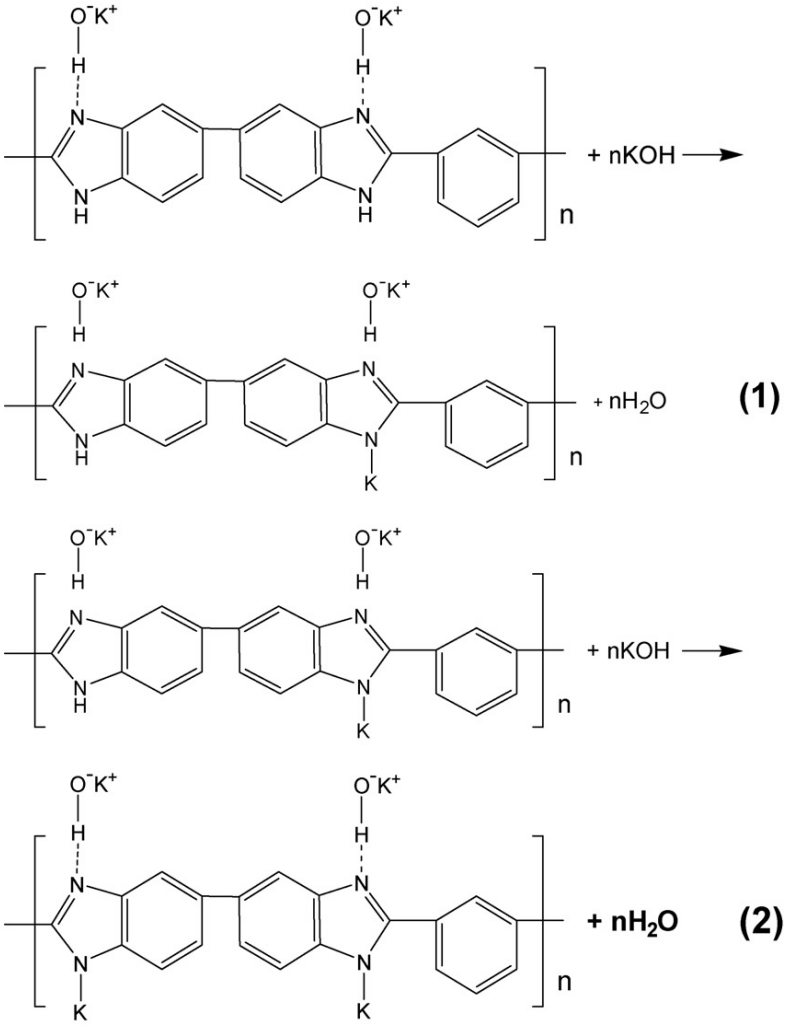

(a)

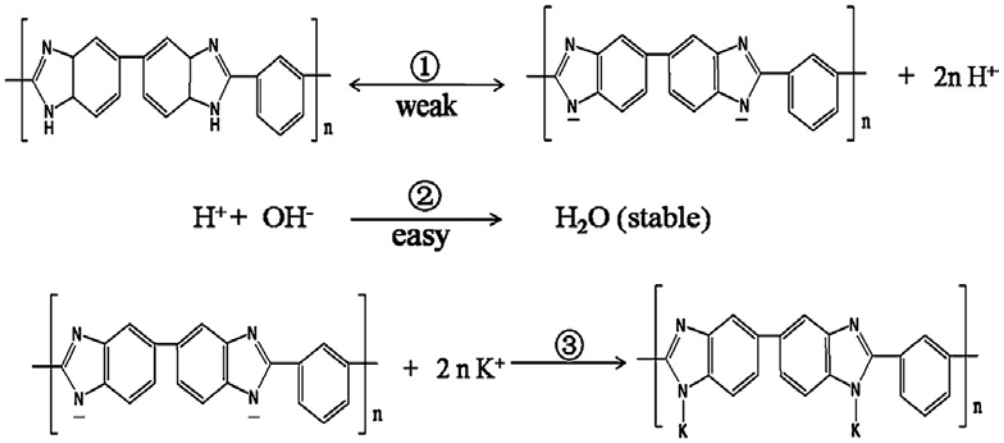

(b)

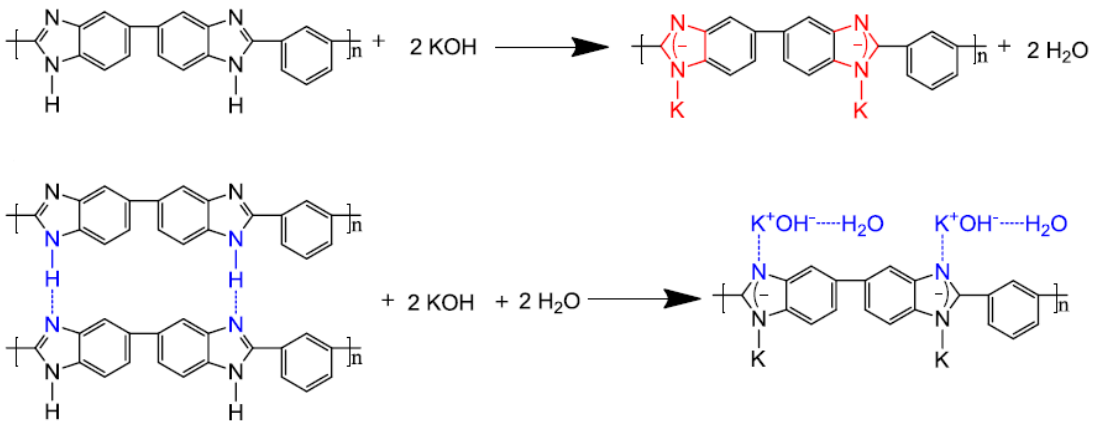

(c)

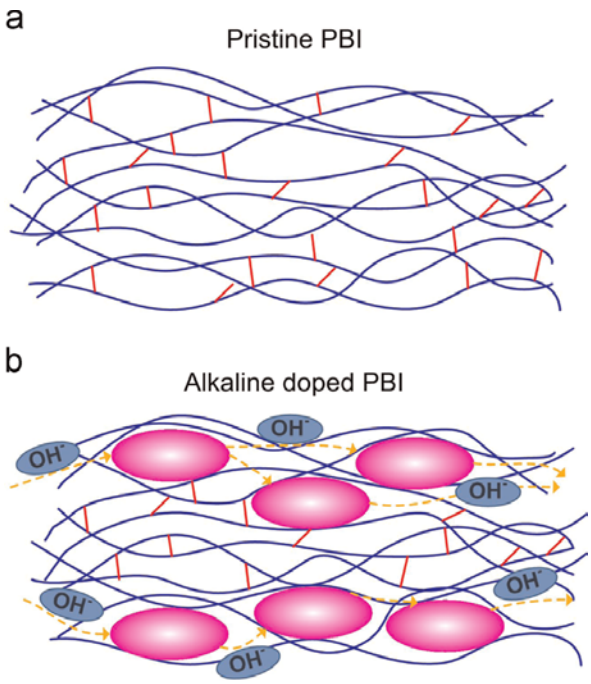

(d)

Fig. 2 (a) The scheme of combination between KOH and -NH- [39]. (b) The possible combination mechanism in details [47]. (c) The possible reaction during the doping process: neutralization reaction and the hydrogen bonds before and after the doping process [45]. (d) Schematic of the pristine PBI membrane and alkali-doped PBI membrane [45]. Reproduced with permission from Elsevier.

In a fuel cell system, positively or negatively charged ions act as charge carriers to

form the ionic current by transporting through ion exchange membranes. In alkali-doped PBI membranes, there are free K^+ and OH^- in the PBI matrix, as well as bonded K^+ and OH^- in the PBI skeleton, creating an anion-cation co-existing system in the PBI membrane after doping. To determine the charge carrier for the ion exchange membrane, An et al. [57] designed an experimental setup and determined the charge carrier of the three different types of commercial membrane, i.e., AEM (A201), CEM (Nafion 211), and NaOH-doped PBI membrane, as shown in Figs. 3a and 3b. It was found that the Na^+ flux through the AEM was almost zero at the whole current density region; while, Na^+ fluxes through the CEM and NaOH-doped PBI membrane were, respectively, 32% and 28% of the theoretical Na^+ flux, meaning that OH^- fluxes through the CEM and NaOH-doped PBI membrane are 68% and 72% of the total ionic current, respectively. Hence, it was indicated that both Na^+ ions and OH^- ions contributed to the ionic current, but the main charge carrier was the OH^- ion.

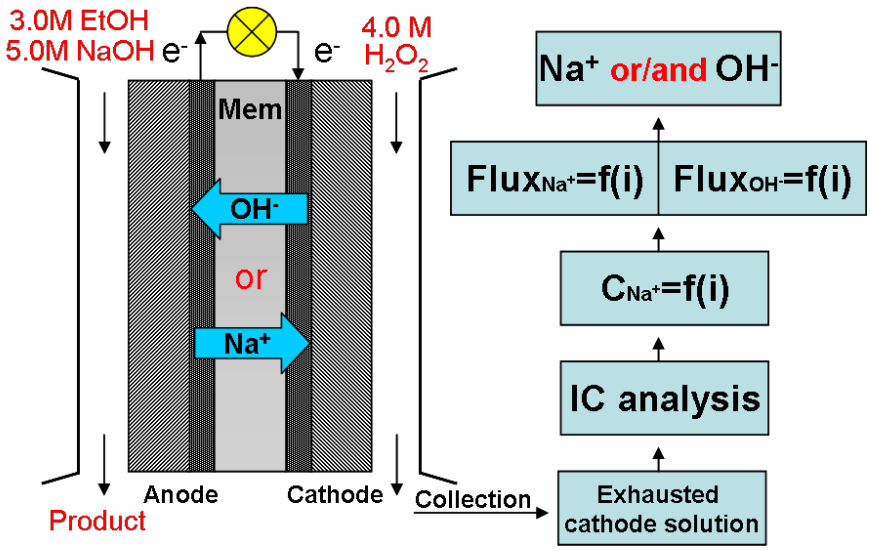

176

177 (a)

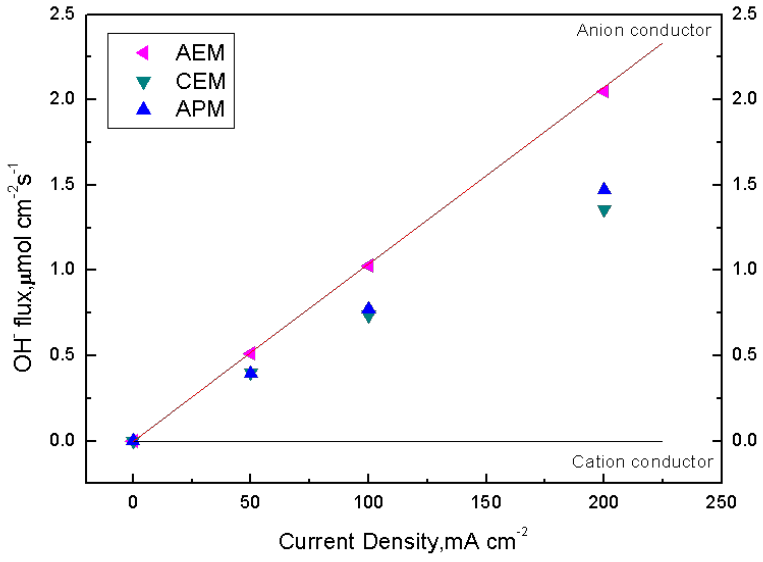

178

179 (b)

180 Fig. 3 (a) Experimental setup and flow chart [57]. (b) Variations in the Na^+ flux

181 through each of three membranes with current density [57]. Reproduced with

182 permission from The Royal Society of Chemistry.

183 **3. Stability of the alkali-doped polybenzimidazole membrane**

The physiochemical properties of ion exchange membranes can significantly affect the fuel cell performance and thus much attention has been paid to the physiochemical characterizations of alkali-doped PBI membranes. This section will summarize and discuss the past research on the thermal and mechanical properties, as well as liquid uptake.

3.1. Thermal stability

The thermal stability of an ion exchange membrane during fuel cell operation is an important property, which significantly affects the stability and durability of the fuel cell system. Radically different from the conventional functional groups based AEMs, the striking feature of the utilization of the PBI membranes fabricated in fuel cells is that they are capable to be operated at a high temperature due to the good thermal stability [35, 36]. After doping with an alkali, however, many physiochemical properties will be changed, such as the ionic conductivity. For this reason, much attention has paid to the thermal stability of alkali-doped PBI membranes via thermogravimetric analysis [38, 48-52]. For example, An et al. [52] conducted the thermogravimetric analysis of three types of commercial membrane, i.e., AEM (Tokuyama A201), cation exchange membrane (CEM: Nafion 211), and NaOH-doped PBI membrane. It was found that among the three membranes, the NaOH-doped PBI membrane showed the comparable thermal stability, both of which were superior than

that of AEM. The NaOH-doped PBI membrane did not exhibit significant degradation when the temperature was over 570^{o}C, and only 30% of the total weight of the membrane was lost at 800^{o}C. Lou et al. [48] investigated the thermal stability of NaOH-doped PBI membranes via the thermogravimetric analysis and found that the retention properties and the water content were slightly increased after doping. It was also found that at temperatures higher than 500°C, a severe weight loss occurred due to the generation of carbon dioxide. Hou et al. [38] evaluated the thermal stability of KOH-doped PBI membrane via TGA and DTA from room temperature to 800^{o}C. They found that the KOH-doped PBI membranes offered reliable thermal stability up to 800^{o}C, which was better than Nafion membranes and quaternary ammonium (QA) based AEMs. In summary, the use of alkali-doped PBI membranes has successfully removed the barrier that limits AEMFCs to be operated at temperatures higher than 60^{o}C.

3.2. Mechanical stability

Excellent mechanical property is crucial for ion exchange membranes to go through harsh processes during fuel cell assembly and operation. Previous publications indicated that even the pristine PBI membrane did not receive any pre-treatment, it still offered a substantial tensile strength [53]. As mentioned earlier, the doping process changes the chemical structure of the membrane, thus definitely changing the

mechanical property. In view of this reason, the mechanical strength of PBI membranes doped with alkali has been widely investigated via testing stress-strain curves [38, 45, 49, 50, 52]. For example, An et al. [52] carried stress-strain tests for three kinds of commercial membrane, i.e., AEM (Tokuyama A201), CEM (Nafion 211), and NaOH-doped PBI membrane. It was found that both the CEM and AEM showed much larger tensile strength than the NaOH-doped PBI membrane, suggesting that the NaOH-doped PBI membrane had the worst mechanical property. It was explained that the mechanical strength of pristine PBI membrane was dominated by the hydrogen bond between –N= and –NH– groups; however, doping the PBI membrane with an alkali was beneficial for the formation of the hydrogen bonds between –N= and alkali, leading to the decrease of molecular cohesion in the NaOH-doped PBI membrane. In addition, introducing the alkali into the substrate of the membrane would reduce the molecular interaction force due to the increasing separation distance. For these reasons, the tensile strength of the NaOH-doped PBI membrane is inferior comparing to the pristine PBI membrane. Zeng et al. [45] also investigated the mechanical property of the PBI membrane doped with alkali comparing to the PBI membrane via measuring the tensile-strain curves. It was found that when the tensile strength reached 92.98 MPa, the pristine PBI membrane broke with an elongation of 5.6%, suggesting that the mechanical strength of pristine PBI

membrane is superior. After doping with an alkali, the tensile strength of breaking was significantly decreased with increasing the KOH concentration. They explained that the original hydrogen bonds were partially cleaved, which decreased molecular cohesion and deteriorated the mechanical strength of the membrane. However, the tensile strength of KOH-doped PBI membranes was still higher than functional groups based AEMs. Hou et al. [38] evaluated the mechanical stability of KOH-doped PBI membranes and determined that the elongation at break and tensile strength and were 20.07% and 7.7 MPa, respectively. They found that those results were lower than the pristine PBI membrane, but comparable with H_3PO_4-doped PBI membranes and some QA-based AEMs. In summary, although the mechanical property of the PBI membrane is lowered to some extent after doping, the alkali-doped PBI membranes have still better mechanical property than Nafion membranes and AEMs do.

3.3. Liquid uptake

The liquid uptake of alkali-doped PBI membranes is an important parameter that directly links with the ionic conductivity. Generally, a higher liquid uptake of the ion exchange membrane will result in a higher ionic conductivity. Nevertheless, the mechanical stability degraded seriously resulting from dimensional changes derived from too high liquid uptake [55]. To determine the liquid uptake, the alkaline doping process of the PBI membrane samples generally lasted for around ten days in order to

make sure that the process was accomplished [45]. So far, the liquid uptake of alkali-doped PBI membranes have been extensively investigated [45, 48, 50, 51, 52, 54]. The liquid uptake of alkali-doped PBI membrane is generally determined by

$$\varphi = \frac{m_w - m_d}{m_d} \times 100\% \quad (1)$$

where m_w denotes the mass of the hydrated membrane (in alkaline solution) and m_d denotes the mass of the dry membrane. An et al. [52] determined the liquid uptakes of three kinds of commercial membrane, i.e., AEM (Tokuyama A201), CEM (Nafion 211), and NaOH-doped PBI membrane. It was found that the liquid uptakes of the NaOH-doped PBI membrane and the AEM were much higher than that of the CEM. In fact, it is the main reason that the NaOH-doped PBI membrane had the worst mechanical property. In addition to the liquid uptake, there are two other uptakes, i.e., water uptake and alkali uptake. Zeng et al. [45] studied the water uptake and alkali uptake of KOH-doped PBI membranes immersed in various KOH concentrations at room temperature. It was found that the alkali uptake and water uptake were low as the PBI membranes were doped with low-concentration KOH solutions; while, the alkali uptake and water uptake were likely to increase linearly as the KOH concentration was higher than 1.0 M. It was also found that when the KOH concentration was further increased to 8.0 M, the PBI membranes were crushed or dissolved in the alkaline solution. It should be noted that there are some differences in

279 the uptakes of alkali-doped PBI membranes, which is probably attributed to the
280 different molecular weight/structure, membrane thickness of the samples, as well as
281 different alkalis [45].

282 **4. Strategies to improve the ionic conductivity of alkali-doped polybenzimidazole**
283 **membranes**

284 The most important function of the ion exchange membrane is to transport ions
285 (charge carrier) through the membrane from one electrode to the other. Hence, the
286 ionic conductivity is an important parameter and has been extensively examined [37,
287 38, 39, 41, 45, 47, 48, 49, 50, 52]. The ionic conductivity was generally determined
288 by Ohm's law:

289 $$\sigma = \frac{d}{R \cdot S} \quad (2)$$

290 where σ is the ionic conductivity (S cm^{-1}), d is the thickness of the membrane
291 (cm), R is the membrane resistance (Ω), and S is the effective area of the
292 membrane (cm^2). In addition, the operating parameters can also affect the ionic
293 conductivity of alkali-doped PBI membranes, such as doping time, alkali type, alkali
294 concentration, carbonate concentration, and operating temperature.

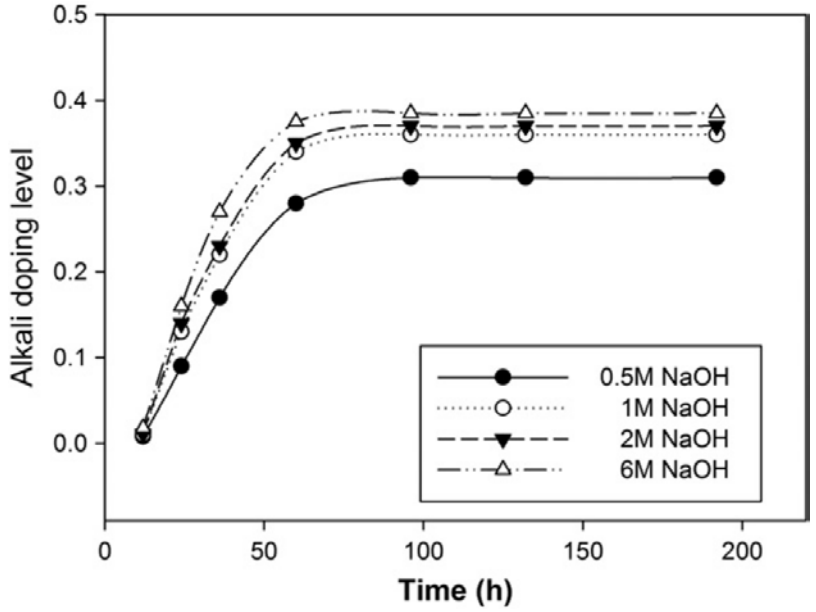

295

296 (a)

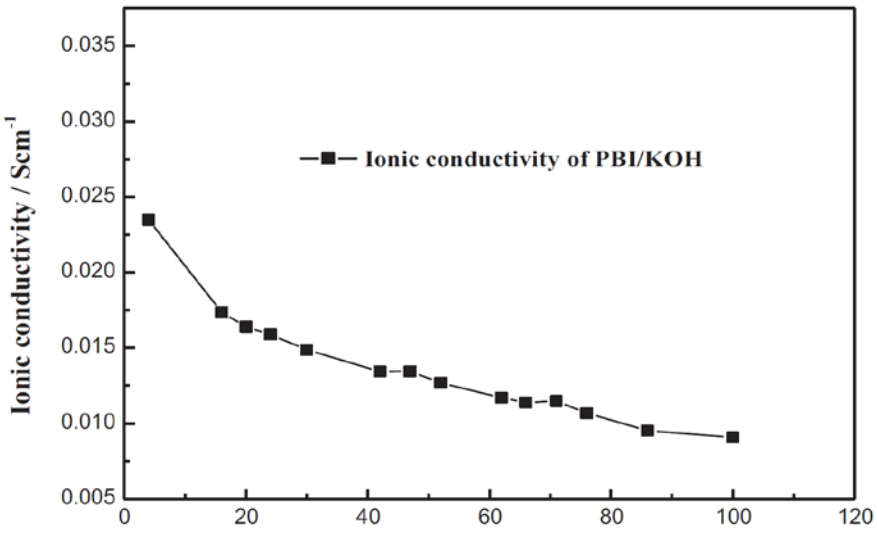

297

298 (b)

299

300

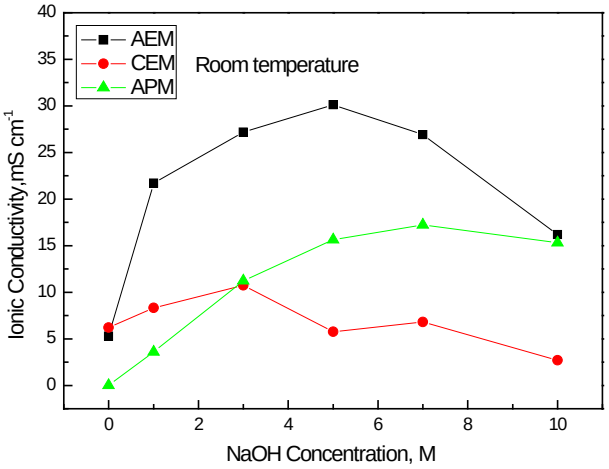

(c)

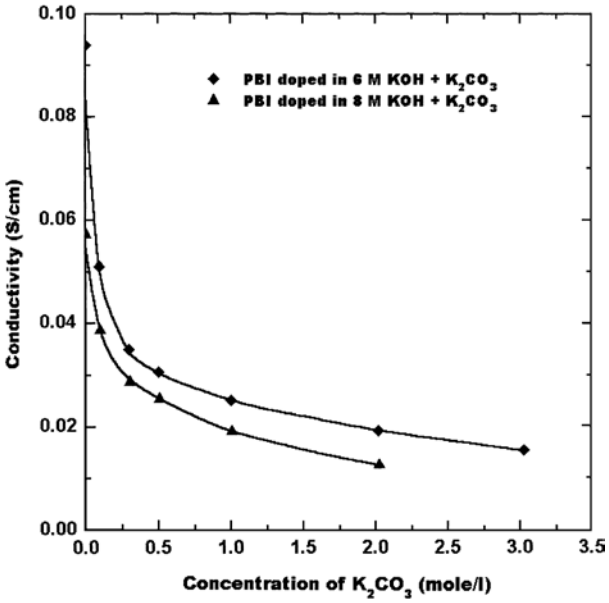

(d)

Fig. 4 (a) Effect of the doping time on the doping level [48]. (b) The ionic conductivity as a function of the time. [47]. (c) Effect of the NaOH concentration on the ionic conductivity [52]. (d) Variation of the ionic conductivity with the doping electrolyte cocnentration at vairous K_2CO_3 concentrations [37]. Reproduced with permission from Elsevier.

4.1. Effect of the doping time

Luo et al. [48] studied the effect of doping time on the doping level of alkali-doped PBI membranes and the results were presented in Fig. 4a. They defined the alkali doping level as the ratio between the weight of doped alkali and the weight of dried membrane. It was found that the alkali doping level first proceeded rapidly within 50 h and then underwent a slow increment rate. Also, the ion conductivity of the PBI membrane doping with 1.0 M NaOH for 200 h (the doping level is 0.37) is 2.3×10^{-2} S cm^{-1} at room temperature. Xing et al. [37] studied the effect of doping time on the optimal alkali concentration and found that the optimal alkali concentration that results in the highest conductivity was increased with the doping time. For example, the optimal concentrations of sodium hydroxide are 8.0 M and 12.0 M for 0.1-day doping and 12-day doping, respectively. It was also found that if the doping time was longer than ten days, the ionic conductivity of the membrane became stable. They explained that the membrane was saturated with the alkali, therefore the ionic conductivity was stable. Hou et al. [39] prepared the alkali-doped PBI membranes by immersing the pristine PBI membrane in 6.0 M KOH at room temperature. Afterwards, the results showed that the doping equilibrium was reached after about 7-day doping. In addition, they conducted the durability test of the KOH-doped PBI membrane by measuring its ionic conductivity at room temperature for 100 h [47]. As

329 shown in Fig. 4b, the initial ionic conductivity of the KOH-doped PBI membrane was
330 2.3×10^{-2} S cm^{-1}. After that, the ionic conductivity of the KOH-doped PBI membrane
331 was gradually degraded with the doping time. After 100-h doping, the ionic
332 conductivity was decreased from 2.3×10^{-2} S cm^{-1} to 1.0×10^{-2} S cm^{-1}, and the
333 degradation rate was 1.3×10^{-4} S cm^{-1} h^{-1}.

334 **4.2. Effect of the alkali type**

335 The alkaline strength has a remarkable influence on the conductivity of the PBI
336 membranes doped with alkali. Xing et al. [37] studied the influence of alkali type on
337 the ionic conductivity and found that it was increased with the strength of the alkaline
338 agent (LiOH < NaOH < KOH). Specifically, the highest conductivity was achieved
339 when doped with KOH and the poorest conductivity was obtained when doped with
340 LiOH. It was also found that the change in the ionic conductivity with the electrolyte
341 concentration also depends on the alkali type. Hence, it is the main reason that KOH
342 is widely used to dope with the PBI membrane.

343 **4.3. Effect of the alkali concentration**

344 An et al. [52] investigated the effect of the NaOH concentration that varied from 0
345 M to 10.0 M on the ionic conductivity of the NaOH-doped PBI membranes, as shown
346 in Fig. 4c. It was found that as the NaOH concentration enhanced, the ionic
347 conductivity was increased first and then decreased, leading to a peak ionic

conductivity. It was explained that once an ion exchange membrane was soaked in an alkaline solution, the generation of alkali-doped free volumes could transport ions under an electric field. Under this circumstance, transporting ions through the alkali-doped free volumes was much easier than through the functional groups. Therefore, the ionic conductivity of PBI membrane in 1.0 M NaOH (3.6 mS cm^{-1}) was better than that of PBI membrane in DI water (0.006 mS cm^{-1}), indicating that the alkali-doped free volumes made subtotal contribution to the ionic conductivity. Nevertheless, the ionic conductivity became lower when the NaOH concentration was higher than 7.0 M, which was ascribed to the increasing viscosity of the alkaline solution and the reducing ionic mobility. Hence, 7.0 M was the optimum alkali concentration, resulting in the maximum conductivity. In summary, a trade-off need to be made between the positive effect of the higher alkali concentration doping and the negative effect of the viscosity increasing in the alkali-doped free volumes of the membrane. Similarly, Xing et al. [37] found that the highest conductivities of PBI membranes doped with alkali were obtained when doping with 8.0-M KOH, 6.0-M NaOH, and 4.0-M LiOH, respectively. Zeng et al. [45] found that the conductivity of the PBI membrane was ultra-low when doping with 0.5 M KOH; while, a promotion in the KOH concentration significantly upgraded the ionic conductivity of PBI membranes doped with alkali.

4.4. Effect of the carbonate presence

Xing et al. [37] conducted the doping process in the mixed solution (KOH and K_2CO_3) and investigated its effect on the ionic conductivity, as shown in Fig. 4d. It was found that like doping in the alkaline solution, the ionic conductivity after 10-min doping was lower than that after 20-day doping. It was also found that the ionic conductivity after doping in the mixed solution (KOH and K_2CO_3) was decreased from 0.095 S cm^{-1} to 0.016 S cm^{-1} as the K_2CO_3 concentration was increased from 0 M to 3.0 M. Although the involvement of K_2CO_3 much decreased the ionic conductivity of the membrane, even at a high K_2CO_3 concentration (3.0 M), the membrane still had an ionic conductivity of 0.016 S cm^{-1}, which was better than that of the Nafion 117 membrane (0.012 S cm^{-1}).

4.5. Effect of the temperature

The most striking feature of the utilization of the alkali-doped PBI membranes in fuel cells is to allow fuel cells to be operated at higher temperatures (> 60^{o}C generally). The effects of operating temperature lie not only on the electrochemical kinetics, but also on the mass/charge transport, including the ion transport through the membrane, i.e., ionic conductivity. Hence, the effect of the operating temperature on the conductivity of alkali-doped PBI membranes has been extensively investigated [37, 45, 48, 52]. In principle, the ionic conductivity of alkali-doped PBI membranes

increases with the increasing temperature, which is attributed to the higher ion mobility. An et al. [52] studied the influence of temperature on the conductivities of the three kinds of commercial membrane in the 5.0 M NaOH solution, i.e., AEM (A201), CEM (Nafion 112), and NaOH-doped PBI membrane, as shown in Fig. 5a. It was found that promoting the operating temperature resulted in almost linearly increasing the ionic conductivities of the three membranes. Specifically, as the operating temperature increased from 23ºC to 60ºC, the ionic conductivities of the AEM, CEM and NaOH-doped PBI membrane was increased from 30.1 mS cm^{-1}, 5.6 mS cm^{-1} and 15.7 mS cm^{-1} to 54.9 mS cm^{-1}, 11.4 mS cm^{-1} and 33.7 mS cm^{-1}, respectively. It was explained that on one hand, a higher temperature accelerated the molecular motions, promoting the ionic transport of the functional groups. On the other hand, elevating the temperature increased the ionic mobility in alkali-doped free volumes, contributing to the increased ionic conductivity. In addition, it was apparent that the activation energy of the three membranes was comparable, suggesting that the three membranes had the analogous ionic conducting mechanism. Lou et al. [48] explored the effect of the operating temperature on the ionic conductivity of PBI membranes doped with alkali. It was found that the ion conductivity of the PBI membrane doped with alkali was significantly enhanced with the operating temperature. Particularly, the ion conductivity of alkali-doped PBI membrane was

increased from 2.3×10^{-2} S cm^{-1} to 7.3×10^{-2} S cm^{-1} when the temperature boosted from room temperature to 100°C. Zeng et al. [45] also found that the ionic conductivity increased with the temperature. The highest ionic conductivity, 96.1 mS cm^{-1} at 90ºC, was achieved when the PBI membrane doping with 6.0 M KOH. They explained that on one hand, the intermolecular interaction was weakened with the increased temperature, leading to an incompact structure and enlarged free volumes; On the other hand, the water uptake of the membrane was enhanced with the temperature, further boosting the ionic conductivity. It was found that the activation energy was 23.22 kJ mol^{-1}, 16.92 kJ mol^{-1}, 16.00 kJ mol^{-1}, 15.87 kJ mol^{-1} when the PBI membrane was doped in 0.5 M KOH, 2.0 M KOH, 4.0 M KOH and 6.0 M KOH, respectively. It was also indicated that the activation energy values were similar to the PBI membrane doped with acid, implying that the transport mechanism was similar, i.e., the Grotthuss mechanism. Xing et al. [37] studied the effect of the doping temperature on the ionic conductivity of the membrane in the mixed solution (KOH + K_2CO_3), as shown in Fig. 5b. It was found that increasing the doping temperature was beneficial for enhancing the ionic conductivity of the membrane doped in the KOH solution. For example, the ionic conductivity increased from 0.02 S cm^{-1} to 0.095 S cm^{-1} when increasing temperature from 25ºC to 70ºC. However, it was found that in the case of the membrane doped in the mixed solution (KOH + K_2CO_3), the ionic

conductivity was almost independent of temperature ranging from 30°C to 70°C. It was explained that the different phenomena were caused by the different ion-conduction mechanisms of two membranes.

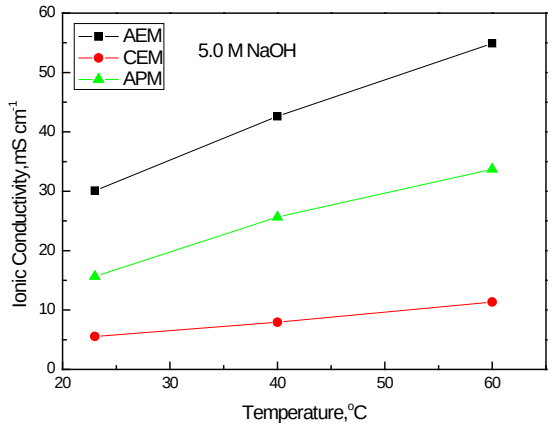

(a)

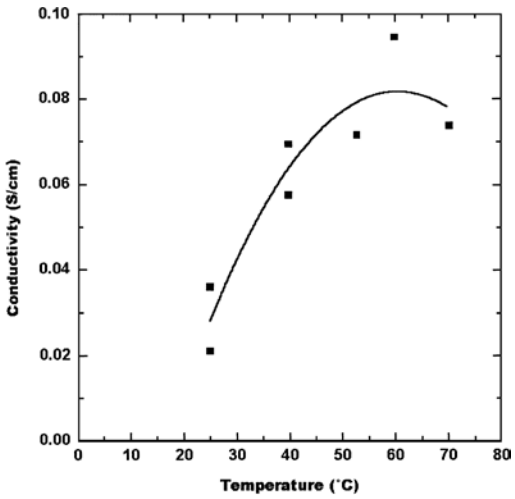

(b)

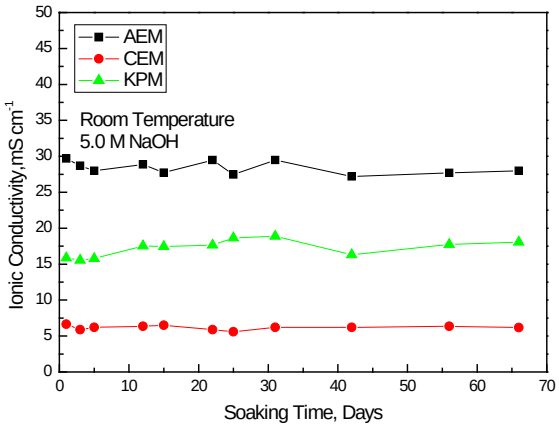

(c)

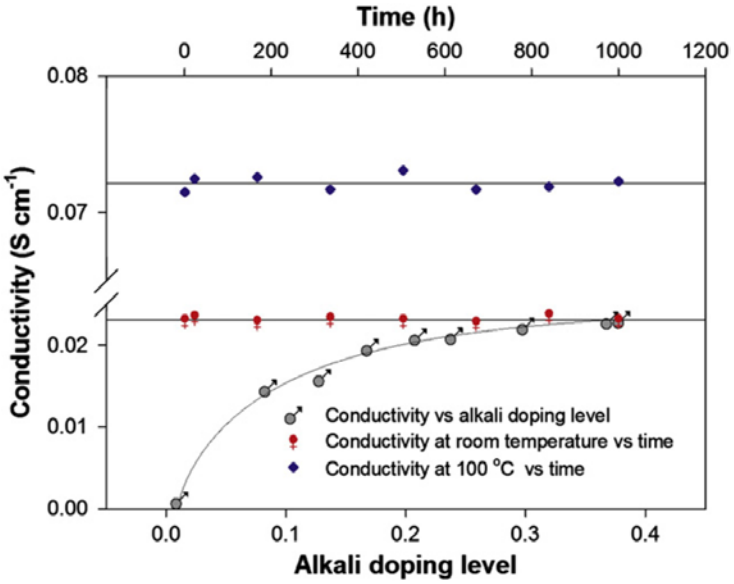

(d)

Fig. 5 (a) Effect of the temperature on the ionic conductivity [52]. (b) Variation of the conductivity of the KOH-doped PBI memrbane with the temperature [37]. (c) Effect of the soaking time on the ionic conductivity [52]. (d) Ion conductivities of the alkali-doped PBI membrane in 1.0 M NaOH [48]. Reproduced with permission from Elsevier.

4.6. Effect of the soaking time

It was claimed that exposing a functional groups based AEM in a concentrated alkaline solution for a long time is potential to cause severe decomposition of the functional groups, thus degrading the ionic conductivity. For this reason, the effect of the soaking time on the ionic conductivity of alkali-doped PBI membranes has been investigated [48, 52]. An et al. [52] examined the conductivity of NaOH-doped PBI membranes soaked in 5.0 M NaOH, as shown in Fig. 5c. It was shown that after being immersed in 5.0 M NaOH for a long period of 70 days, the ionic conductivity of the membrane remained almost the same. It was indicated that the soaking time did not obviously influence the ionic conductivity of alkali-doped PBI membranes. Lou et al. [48] examined the ionic conductivity of PBI membranes doped with alkali, as shown in Fig. 5d, and found that the ionic conductivity was almost unchanged in 1.0 M NaOH at room temperature and 100°C for 1000 h. It was indicated that the PBI membrane doped with alkali was stable in alkaline media at temperatures up to 100°C. In summary, the utilization of alkali-doped PBI membranes in AEMFCs will broaden the operating temperature range and thus improve the cell performance.

5. Application of alkali-doped polybenzimidazole membranes in fuel cells

5.1. Fuel permeability

Fuel permeability of the ion exchange membranes is an important parameter that

459 significantly affects the fuel cell performance, resulting from the fact that fuel
460 transporting through the membrane (fuel crossover) may cause two technical
461 problems. Firstly, fuel may be oxidized with the help of the cathode electrocatalysts to
462 form the parasitic current, leading to a mixed potential on the cathode. Secondly, the
463 fuel crossover definitely leads to a waste of fuel, lowering the fuel utilization
464 efficiency. Hence, the membrane candidate for fuel cells should have low fuel
465 permeability. Therefore, the fuel permeability of PBI membranes doped with alkali
466 have been extensively examined [38, 39, 45, 51, 52, 56], such as methanol and
467 ethanol. For example, Hou et al. [38, 39] also measured methanol and ethanol
468 permeability of KOH-doped PBI membranes at room temperature. It was shown that
469 methanol and ethanol permeability were 2.6×10^{-7} cm^2 s^{-1} and 6.5×10^{-7} cm^2 s^{-1},
470 respectively. Zeng et al. [45] investigated methanol and ethanol permeability of the
471 pristine and KOH-doped PBI membranes, respectively. The results showed that the
472 pristine PBI membrane exhibited a limited methanol and ethanol permeability due to
473 the fact that it has a low liquid uptake. After doping in 6.0 M KOH, the methanol and
474 ethanol permeability was significantly increased due to the reduced intermolecular
475 interaction rendered by the established ionic channels. It was also found that the
476 methanol permeability was higher than ethanol due to the fact that the hydrated
477 molecular size of methanol is smaller, resulting in a high transport rate through the

KOH-doped PBI membrane. Leykin et al. [56] developed a new method to determine the ethanol permeability of polymeric membranes in alkaline media. By using this method, the ethanol permeability (8.6×10^{-8} cm^2 s^{-1}) was obtained in 3.0 M KOH, which was further decreased with the alkali concentration. In addition, they concluded that this method could be expanded to measuring alcohol permeability of polymeric membranes in acidic conditions and various aqueous solutions. Recently, An et al. [52] determined the ethanol and NaOH permeability of three types of commercial membrane at room temperature, i.e., AEM (Tokuyama A201), CEM (Nafion 211), and NaOH-doped PBI membrane by using a home-made diffusion cell. It was found that the ethanol permeability through the three membranes was similar (1×10^{-7} cm^2 s^{-1}); while, the NaOH permeability through the NaOH-doped PBI membrane was as high as 19.83×10^{-8} cm^2 s^{-1}, but the NaOH permeability through the CEM and AEM was relatively lower, i.e.: 2.541×10^{-8} cm^2 s^{-1} and 3.778×10^{-8} cm^2 s^{-1}, respectively. It was explained that the both AEM and CEM had functional groups, which could impede the ion transport due to the charge repulsion.

5.2. Single-cell performance

As mentioned earlier, alkali-doped PBI membranes offer the good thermal stability and high ionic conductivity. As such, this type of membrane has been extensively used in fuel cells running on various fuels, such as hydrogen [37, 50, 54, 58], methanol [38,

51], ethanol [39, 46, 47], ethylene glycol [40], glycerol [41], formate [42], and borohydrides [43]. This section will summarize past efforts in the performance characterization of fuel cells that use alkali-doped PBI membranes.

5.2.1. Hydrogen

As summarized in Table 1, it can be seen that although this type of fuel cell is still an emerging power-supply technology, the maximum power density has been substantially promoted in recent years. Specifically, Xing et al. [37] fabricated and tested a hydrogen/oxygen fuel cell by employing a KOH-doped PBI membrane with a thickness of 40 μm. It was found that the fuel cell exhibited a current density of 620 mA cm^{-2} at a voltage of 0.6 V, which was similar to that achieved by a PEMFC using a Nafion 117 membrane. Zarrin et al. [50] developed a durable and highly ion-conductive KOH-doped porous PBI membrane for AEMFCs, as shown in Fig. 6a, in which the porosity was introduced, enhancing the attraction of the KOH solution and thus increasing the ionic conductivity. It was found that the ionic conductivity and cell performance yielded by using the KOH-doped porous PBI membrane with a porosity of 0.7 were around two times higher than those achieved by using the commercial Fumapem® FAA membrane. In addition, the KOH-doped porous PBI membrane could maintain the ionic conductivity after a 14-day stability testing; while, the commercial one started to degrade just after 3 hours. It was indicated that the peak

power density achieved by using a KOH-doped porous PBI membrane with a porosity of 0.7 was about 72 mW cm^{-2}, which was 1.8 and 1.5 times higher than those achieved by using a KOH-doped dense PBI membrane (41 mW cm^{-2}) and the commercial FAA membrane (45 mW cm^{-2}), respectively, as shown in Fig. 6b. They demonstrated that the substantial enhancement in performance was ascribed to the fact that the porous structure offered a higher ion transport rate through the membrane. However, a challenging issue associated with the alkali-doped porous/dense PBI membrane is the gradual release of the doped alkali during the fuel cell operation. To address this issue, Zeng et al. [54] proposed and fabricated a KOH-doped sandwiched-porous PBI membrane via a pore-forming method, which renders numerous sponge-like walls and interconnected macropores, enhancing the attraction between the PBI skeleton and the doped alkali, as illustrated in Fig. 6c. It was indicated that both ionic conductivity and alkali retention of the membrane could be substantially enhanced via this approach. It was also demonstrated that the use of this KOH-doped sandwiched-porous PBI membrane in an AEMFC led to an open-circuit voltage (OCV) of 1.0 V and a maximum power density of 544 mW cm^{-2} at 90^{o}C, as shown in Fig. 6d, which was better than that obtained by using the conventional membrane structure. In addition, they also examined the stability of the fuel cell at a current density of 700 mA cm^{-2} and found that the conventional fuel cell exhibited a

dramatic voltage drop just after 5 hours, even to almost zero, which was caused by a progressive release of the doped alkali from the membrane, thereby gradually losing the capability of conducting ions through the membrane. Unlike the conventional one, the sandwiched membrane much improved the stability: the cell voltage was gradually reduced from 0.55 V to 0.1 V, and remained at 0.1 V for another 25 hours. They explained that the performance improvement was attributed to the improved attraction of the doped alkali on the sponge-shaped wall, retarding the release of the doped alkali, and the high ionic conductivity of the sandwiched membrane. It should be noted that the sponge-shaped structure was not capable to completely prevent the release of the doped alkali due to the fact that the cell voltage was gradually decreased over time as a result of a gradual depletion of the doped alkali. They pointed out, however, that this sandwiched membrane could be reused once doped in the KOH solution again. In addition to functioning as an ion exchange membrane, PBI after doping can be used as an ionomer, which not only serves as a binder but also as the ion-conductive pathway.

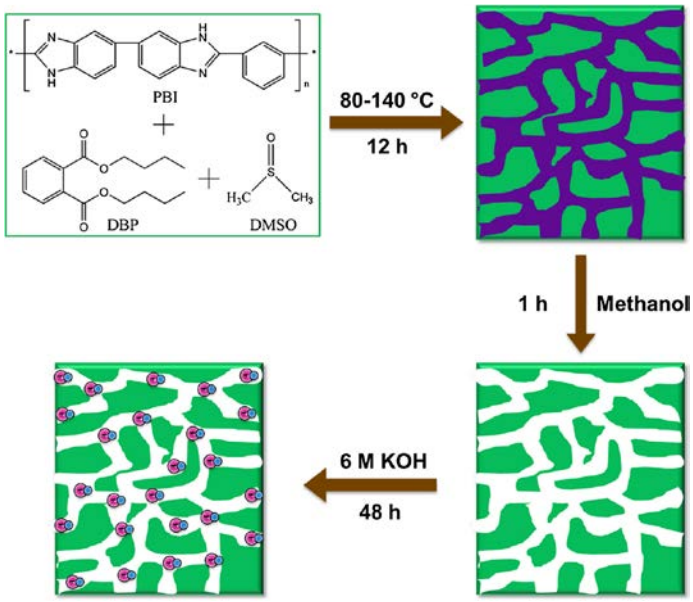
PBI
DBP
DMSO
80-140 °C
12 h
1 h
Methanol
6 M KOH
48 h

(a)

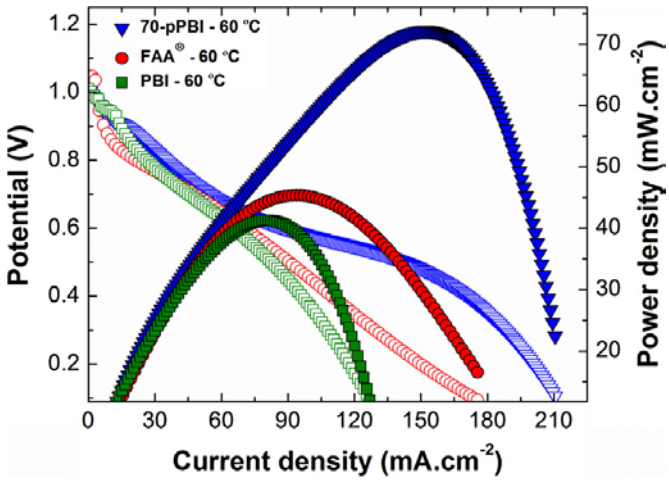
70-pPBI - 60 °C
FAA® - 60 °C
PBI - 60 °C
Potential (V)
Power density (mW.cm-2)
Current density (mA.cm-2)

(b)

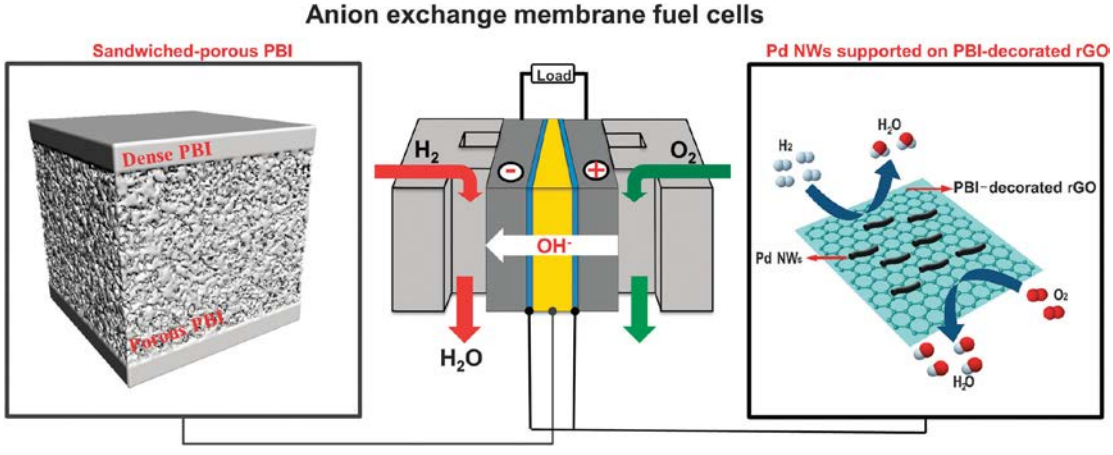
Anion exchange membrane fuel cells
Sandwiched-porous PBI
Dense PBI
Porous PBI
Load
H2
O2
OH-
H2O
Pd NWs supported on PBI-decorated rGO
PBI-decorated rGO
Pd NWs

(c)

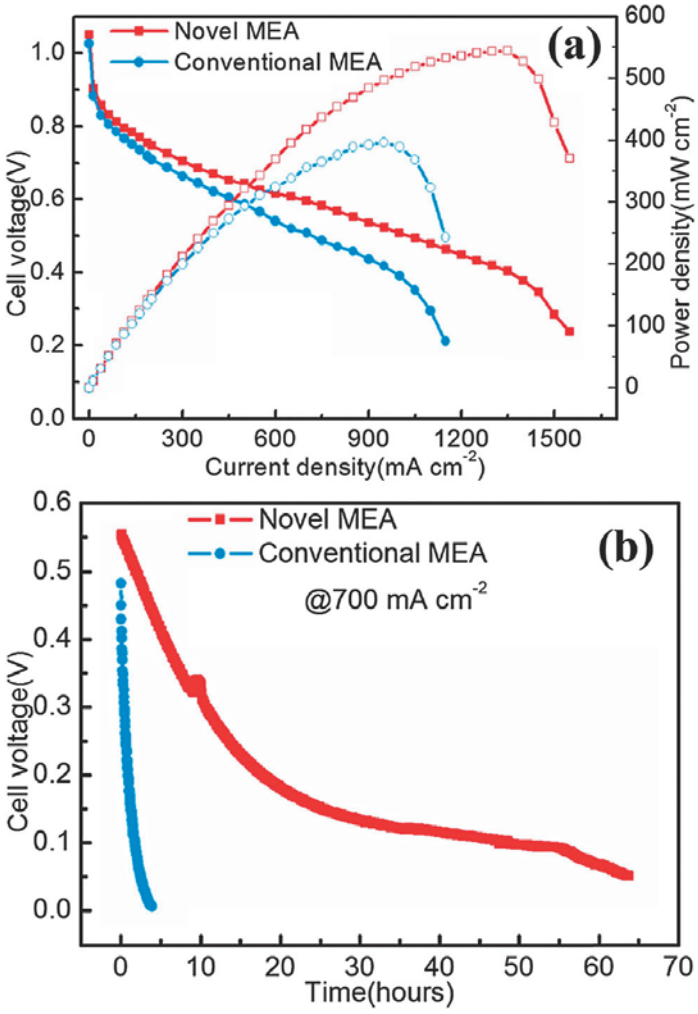

(d)

Fig. 6 (a) The fabrication process of KOH-doped porous PBI membranes [50]. (b) The polarization and power density curves using three membranes [50]. (c) Schematic illustration of a PBI-based membrane electrode assembly and the fuel cell [54]. (d) The polarization and power density curves with the conventional MEA (round symbols) and the novel MEA (square symbols), and the constant current discharging behaviors using the conventional MEA and the novel MEA at a current density of 700 mA cm^{-2} [54]. Reproduced with permission from Elsevier and The Royal Society of Chemistry.

566 Matsumoto et al. [58] developed a well-structured electrocatalyst for AEMFCs,
567 consisting of carbon nanotubes (CNTs) as supporter, KOH-doped PBI ionomer as
568 binder and platinum nanoparticles, in which the CNTs were wrapped by the
569 KOH-doped PBI ionomer at a nanometer thickness and Pt nanoparticles were loaded
570 on the wrapping layer, as shown in Fig. 7a. In principle, the CNTs and the
571 KOH-doped PBI ionomer layer function as electron and hydroxide conductive
572 pathways, respectively, and the large exposed surface of the Pt nanoparticles allows an
573 effective access of hydrogen. Such a triple phase boundary structure with small
574 electrolyte content resulted in a high effective diffusivity and enhanced the
575 electrochemical activity. It was also demonstrated that the use of this electrocatalyst
576 resulted in a peak power density of 256 mW cm^{-2} at 50^{o}C, as shown in Fig. 7b.

577 **5.2.2. Methanol**

578 In addition to hydrogen, the alkali-doped PBI membrane can be used to construct a
579 fuel cell running on various liquid fuels, such as methanol and ethanol [38, 39, 46, 47,
580 51]. For fuel cells running on methanol, Hou et al. [38] fabricated an alkaline direct
581 methanol fuel cell by using a KOH-doped PBI membrane and found that when the
582 cell was fueled with a mixed solution containing 2.0 M methanol and 2.0 M KOH, the
583 OCV was about 1.0 V and the maximum power density was about 31 mW cm^{-2} at
584 90^{o}C, as shown in Fig. 7c. Wu et al. [51] prepared the KOH-doped PBI/CNT

585 nanocomposites as the hydroxide conducting membrane for alkaline direct methanol
586 fuel cells. It was shown that the CNT promoted the ionic conductivity and thus
587 improved the fuel cell performance. It was found that when the fuel cell was operated
588 with 2.0 M methanol + 6.0 M KOH and humidified oxygen, the maximum power
589 densities of 67 mW cm^{-2} and 104 mW cm^{-2} were achieved at 60°C and 90°C,
590 respectively. Li et al. [60] treated the pristine PBI membrane, which was synthesized
591 via a solution casting method, in 2.0 M phosphoric acid and 6.0 M potassium
592 hydroxide solution, respectively, to prepare a PEM and an AEM for direct methanol
593 fuel cells. They also studied the effects of the structure design and operating
594 parameters on the cell power-output, including the methanol concentration, the
595 anolyte flow rate, operating temperature, as well as the hydrophobicity of the
596 micro-porous layer (MPL). It was found that the KOH-doped PBI membrane offered a
597 higher conductivity (21.6 mS cm^{-1}) than the H_3PO_4-doped PBI membrane (7.9 mS
598 cm^{-1}) did at 90°C; while, the two membranes showed the similar methanol
599 permeability on the order of 10^{-7} cm^2 s^{-1}. It was also found that the direct methanol
600 fuel cell with a KOH-doped PBI membrane exhibited a maximum power density of
601 117.9 mW cm^{-2} at 90°C, which was two times higher than that (46.5 mW cm^{-2})
602 achieved by using a H_3PO_4-doped PBI. In addition, they found that when the fuel
603 flow rate was tripled, the fuel cell with a MPL-free electrodes structure resulted in a

604 peak power density of 158.9 mW cm^{-2} at 90°C, as shown in Fig. 7d.

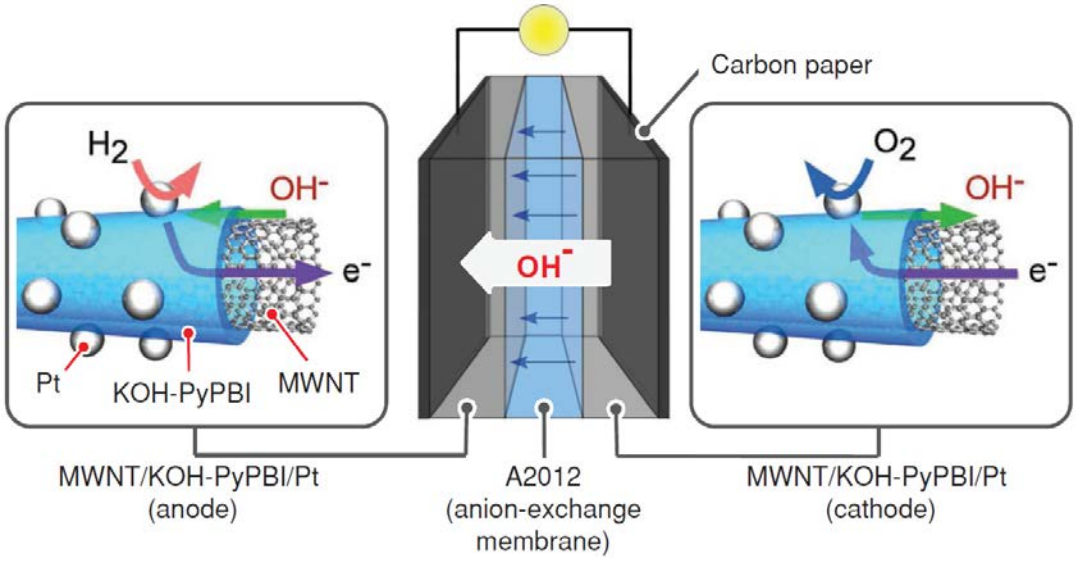

605

606 (a)

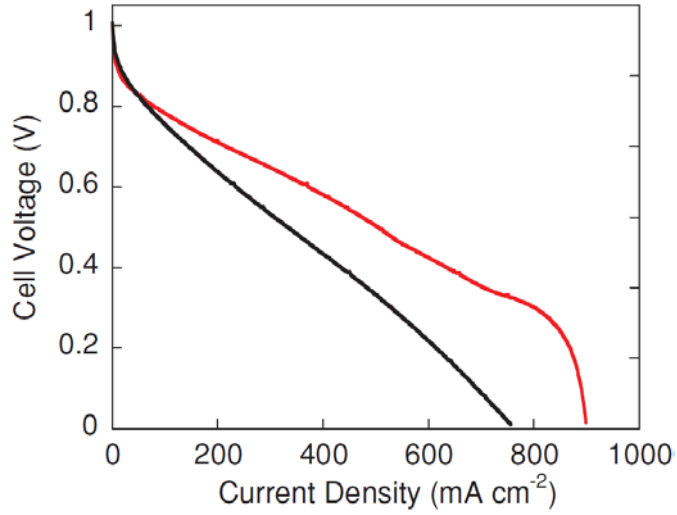

607

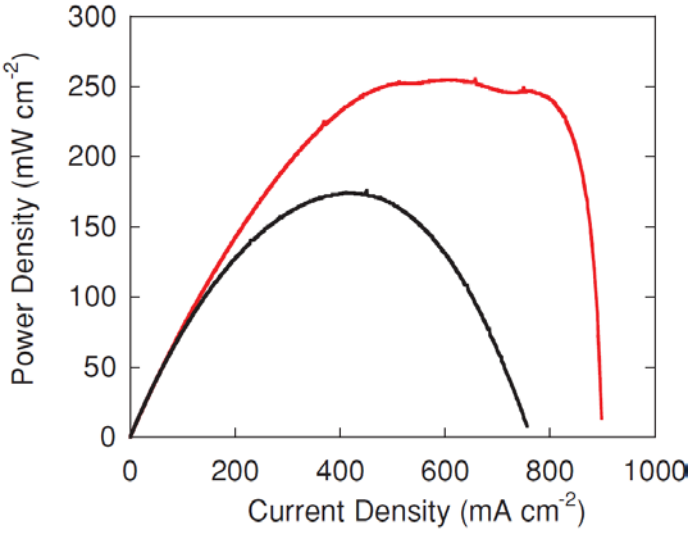

608

609 (b)

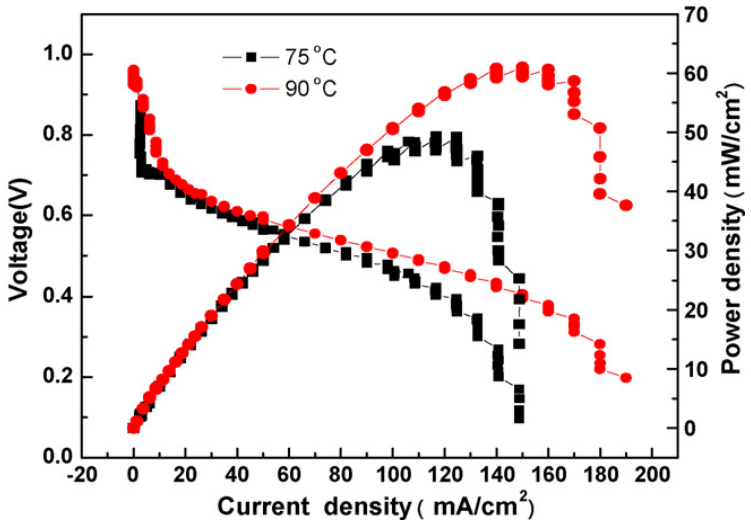

610

611 (c)

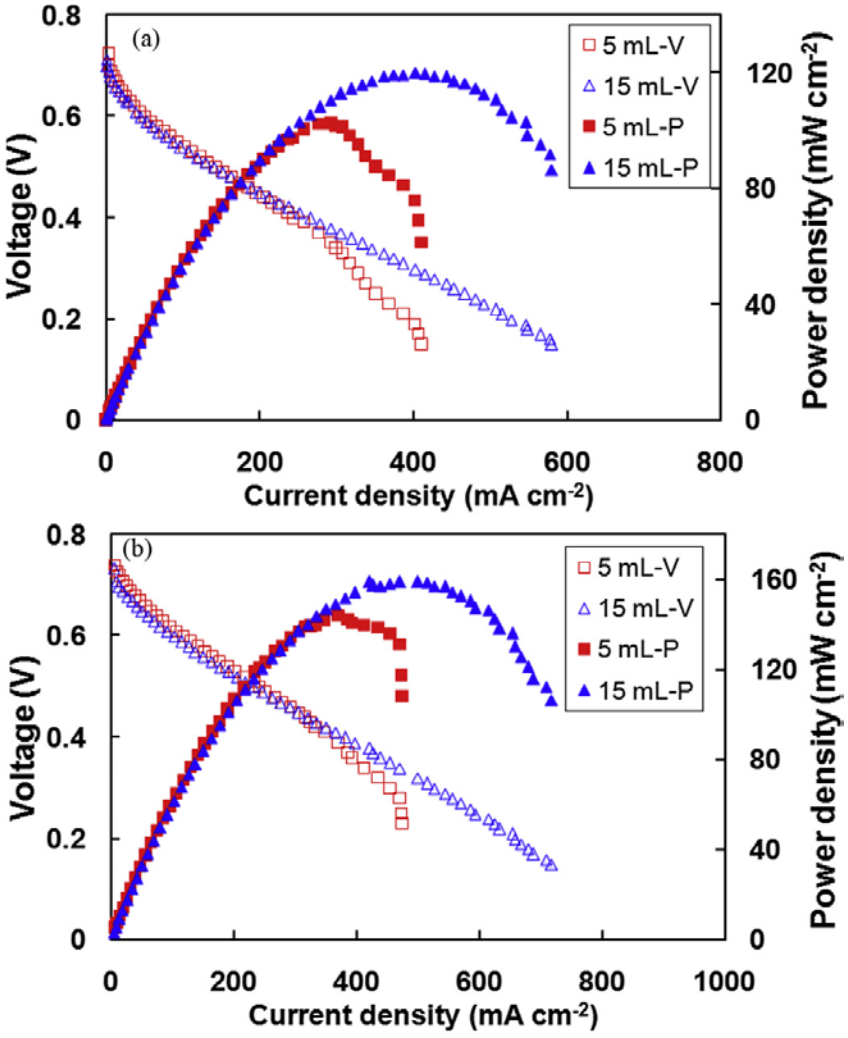

612

613 (d)

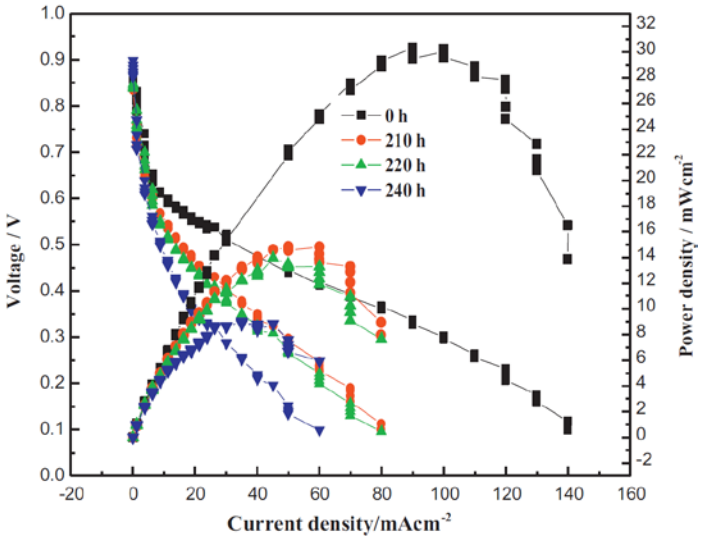

(e)

Fig. 7 (a) Schematic illustration of an anion exchange membrane fuel cell [58]. (b) The polarization and power density curves of the fuel cell (red line: PyPBI cell; black line: AS-4 cell) [58]. (c) The polarization curves of an alkaline direct ethanol fuel cell with alkali-doped PBI membrane at 75°C and 90°C [38]. (d) The performance of direct methanol fuel cells using a KOH-doped PBI membrane and H_3PO_4-doped PBI membrane at 60°C (upper) and 90°C (lower), respectively [60]. (e) The performance of an air-breathing alkaline direct ethanol fuel cell at 60°C [47]. Reproduced with permission from Wiley and Elsevier.

5.2.3. Ethanol

As for fuel cells running on ethanol, Hou et al. [39] developed and fabricated an alkaline direct ethanol fuel cell with a KOH-doped PBI membrane. It was found that

when the cell was operated with 2.0 M ethanol + 2.0 M KOH, the OCVs were 0.92 V at 75^{o}C and 0.97 V at 90^{o}C, respectively, and the maximum power densities were 49.2 mW cm^{-2} at 75^{o}C and 60.9 mW cm^{-2} at 90^{o}C, respectively. Modestov et al. [46] fabricated a membrane electrode assembly (MEA) for alkaline direct ethanol fuel cells, which were prepared by employing non-platinum electrocatalysts and a KOH-doped PBI membrane. It was demonstrated that a peak power density of 100 mW cm^{-2} was obtained at a voltage of 0.4 V at 80^{o}C when using the air as the oxidant and a mixed solution containing 3.0 M KOH + 2.0 M ethanol as fuel. In addition, they also found that the fuel cell operated with pure oxygen resulted in about 10% increment in the current density. Recently, Hou et al. [47] examined the stability of the KOH-doped PBI membrane by assembling an alkaline direct ethanol fuel cell with an air-breathing mode at 60^{o}C, which employed PtRu/C and MnO_2/C as anode and cathode electrocatalysts, respectively. It was shown that a 256-h discharging curve with large voltage fluctuations (> 100 mV) during the whole discharging process. In addition, during the durability test, the polarization and power density curves were collected at 0 h, 210 h, 220 h and 240 h, respectively. It was shown from Fig. 7e that the peak power densities at four operation points were about 30 mW cm^{-2}, 15 mW cm^{-2}, 14 mW cm^{-2} and 9 mW cm^{-2}, respectively, leading to a degradation rate of 0.08 mW cm^{-2} h^{-1}. In addition, they also explained that the voltage fluctuation was attributed to the

use of PtRu/C electrocatalyst on the anode, as the large voltage fluctuation phenomenon disappeared when the PtRu/C catalyst was replaced by the Pd/C electrocatalyst.

5.2.4. Other alcohols

In addition to methanol and ethanol, alkali-doped PBI membranes have been employed in fuel cells running other alcohols. For example, An et al. [40] fabricated an alkaline direct ethylene glycol fuel cell by using a KOH-doped PBI membrane with a thickness of 30 μm, allowing the fuel cell system to be operated at temperatures higher than 60ºC. The fuel cell was fabricated with PdNi/C as the anode electrocatalyst (1.0 mg cm^{-2}) and non-platinum HYPERMEC^{TM} as the cathode electrocatalyst (1.0 mg cm^{-2}). It was shown that a maximum power density of 112 mW cm^{-2} was obtained when operated at 90ºC with a mixed aqueous solution of 1.0 M ethylene glycol and 7.0 M KOH fed into anode at a flow rate of 2.0 mL min^{-1} and dry pure oxygen supplied into cathode at a flow rate of 100 sccm. The replacement of the pure oxygen by the air declined the maximum power density to 92 mW cm^{-2}. Nascimento et al. [41] developed an alkaline direct glycerol fuel cell with a KOH-doped PBI membrane. It was shown that the developed fuel cell could be operating at temperatures as high as 75ºC. In addition, they also investigated the effects of the various operating conditions on the cell performance and determined the

optimal values for the given MEA, including glycerol concentration (1.0 M), KOH concentration (4.0 M), the anolyte flow rate (2.0 mL min^{-1}). Moreover, they compared the three anode electrocatalysts, i.e., Pt/C, PtRu/C, and Pt_3Sn/C and found the PtRu/C and Pt_3Sn/C electrocatalysts showed higher activity to the glycerol oxidation. Furthermore, they systematically investigated the alkali-doped PBI membranes for direct glycerol fuel cells and found that the fuel cell fed with 1.0 M glycerol and 4.0 M KOH led to a maximum power density of 34.2 mW cm^{-2} at 75°C [51].

5.2.5. Solid fuels

The alkali-doped PBI membranes have also been used in fuel cells running on formate [42] and borohydrides [43]. Jiang et al. [42] developed a direct formate fuel cell employing Pd/C (4.0 mg cm^{-2}) and Ag/C (8.0 mg cm^{-2}) as anode and cathode electrocatalysts, respectively, together with a 40-μm KOH-doped PBI membrane. The fuel cell was tested with a mixed solution containing HCOOK + 2.0 M KOH fed into anode at a flow rate of 6.0 mL min^{-1} and pure oxygen as oxidant supplied into cathode at a flow rate of 200 sccm varying from 80°C to 120°C. It was shown that the fuel cell operated with 6.0 M HCOOK resulted in a peak power density of about 160 mW cm^{-2} at 120°C, as shown in Figs. 8a and 8b. Chen et al. [43] synthesized a NaOH-doped porous PBI membrane for direct borohydride fuel cells via water vapor phase inversion process, as shown in Fig. 8c. It was shown that as compared to the Nafion

115 membrane, the membrane showed a higher ionic conductivity. It was also found that the membrane exhibited good chemical stability, which was evidenced by that no weight loss was observed after immersing the membranes in the 3.0 M NaOH solution for 30 days. The fuel cell was tested at 40ºC with the fuel solution containing 1.0 M $NaBH_4$ + 3.0 M NaOH supplied at a flow rate of 0.5 mL min^{-1} and pure oxygen as oxidant provided with a pressure of 0.1 MPa. It was shown that the a peak power density of 262 mW cm^{-2} was achieved in a direct borohydride fuel cell in a direct borohydride fuel cell by using the membrane with a porosity of 0.6, as shown in Fig. 8d, which was much higher than that achieved by using the Nafion 115 membrane. In addition, the direct borohydride fuel cell could discharge at a current density of 200 mA cm^{-2} for about 250 hours without any voltage decay.

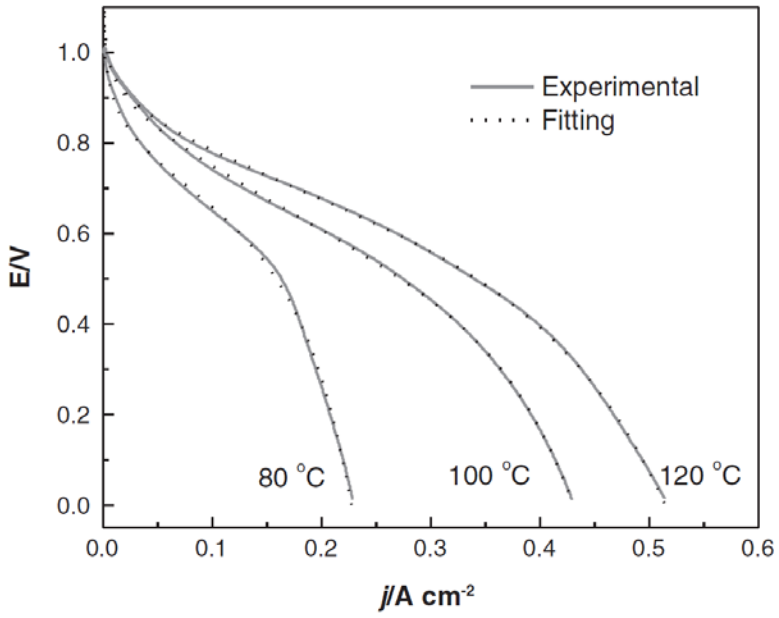

(a)

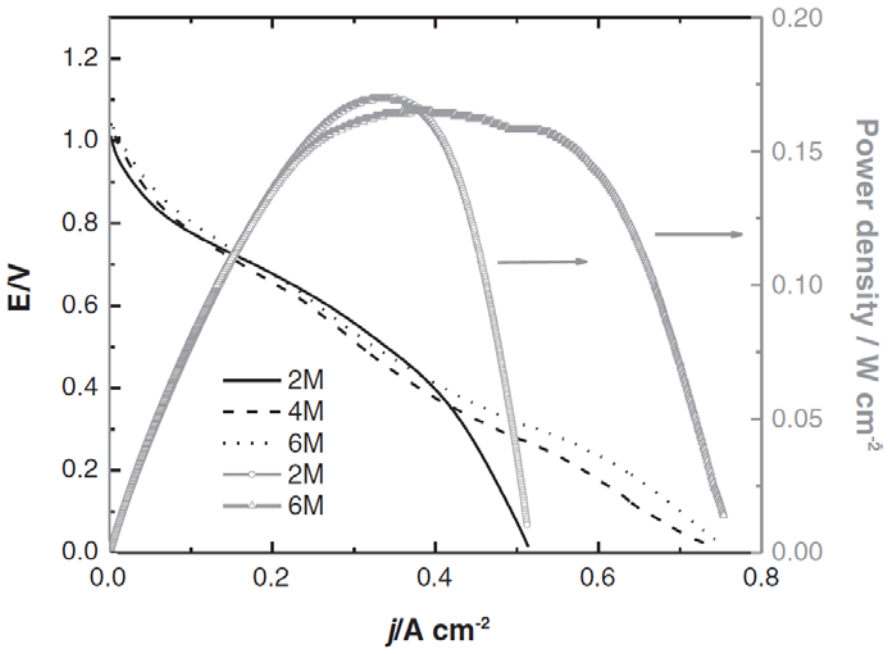

698

699 (b)

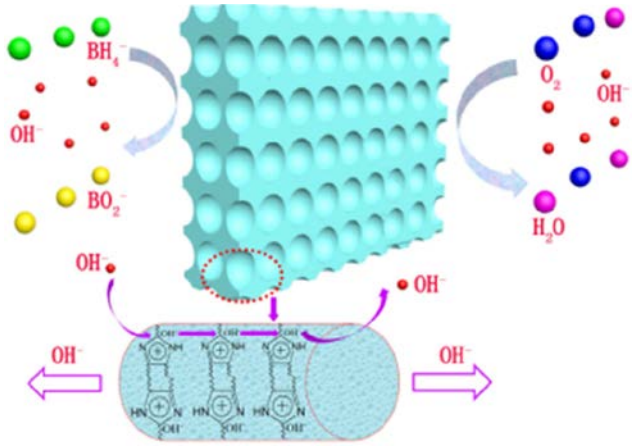

700

701 (c)

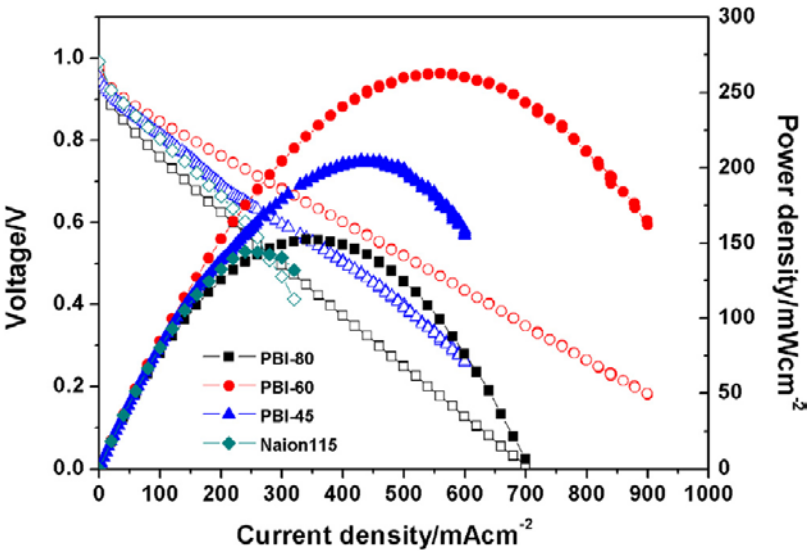

(d)

Fig. 8 (a) Temperatuere dependence of polarization curves for a direct formate fuel cell with a fuel of 2.0 M KOH + 2.0 M HCOOK [42]. (b) HCOOK cocnentration dependence of polarization and power density curves for a direct formate fuel cell at 120ºC [42]. (c) Schematic of the designed membrane [43]. (d) The polarization and power density curves of direct borohydride fuel cells with the prepared membranes [43]. Reproduced with permission from Elsevier.

6. Summary and outlook

As a result of the well-known excellent thermal stability and high ionic conductivity after doping with an inorganic alkali, polybenzimidazole has been recognized as an alternative for anion exchange membranes and has made considerable progress in recent years. The fact that the use of alkali-doped PBI membrane allows anion exchange membrane fuel cells to operate at high temperatures

provides various advantages including fast electrochemical kinetics, low cost, high CO tolerance, facilitating the progress in practical applications. This article provides a review of up-to-date research on the alkali-doped PBI membranes and their applications in fuel cells. Particular attention has been paid to their physiochemical properties and fuel cell performance. It should be mentioned that the stability of the alkali-doped PBI membranes including thermal stability, mechanical stability, and liquid uptake are compared and discussed in details. The past investigations have laid a solid foundation for the basic understanding of how the operating parameters affect the physiochemical properties of alkali-doped PBI membranes and the corresponding fuel cell performance with various fuels. In the race of replacing the anion exchange membranes by the alkali-doped PBI membranes, several critical issues that need to be addressed in the future include: 1) reducing the fuel permeability; 2) enhancing the alkali retention (or reducing the alkali leakage); 3) understanding the mechanisms of mass/ion transport through the membrane; 4) optimizing the sandwiched membrane structure that enables high conductivity, high alkali retention, but low permeability.

Acknowledgements

The authors gratefully acknowledge the financial supports of the Natural Science Foundation of China (No. 51506039) and the Shenzhen Science and Technology Fund (JCYJ20170818093905960).

References

[1] E. Antolini, E.R. Gonzalez, Alkaline direct alcohol fuel cells, J. Power Sources 195 (2010) 3431-3450.

[2] E.H. Yu, X. Wang, U. Krewer, L. Lid, K. Scott, Direct oxidation alkaline fuel cells: from materials to systems, Energy Environ. Sci. 5 (2012) 5668-5680.

[3] L. An, T.S. Zhao, Y.S. Li, Carbon-neutral sustainable energy technology: Direct ethanol fuel cells, Renewable and Sustainable Energy Reviews 50 (2015) 1462-1468.

[4] J.R. Varcoe, P. Atanassov, D.R. Dekel, A.M. Herring, M.A. Hickner, P.A. Kohl, A.R. Kucernak, W.E. Mustain, K. Nijmeijer, K. Scott, T.W. Xu, L. Zhuang, Anion-exchange membranes for electrochemical energy systems, Energy Environ. Sci. 7 (2014) 3135-3191.

[5] L. An, R. Chen, Direct formate fuel cells: A review, J. Power Sources 320 (2016) 127-139.

[6] X. Ren, S.C. Price, A.C. Jackson, N. Pomerantz, F.L. Beyer, Highly Conductive Anion Exchange Membrane for High Power Density Fuel-Cell Performance, ACS Appl. Mater. Interfaces 6 (2014) 13330-13333.

[7] L. An, T.S. Zhao, X.H. Yan, X.L. Zhou, P. Tan, The dual role of hydrogen peroxide in fuel cells, Science Bulletin 60 (2015) 55-64.

[8] G. Merle, M. Wessling, K. Nijmeijer, Anion exchange membranes for alkaline fuel

754 cells: A review, J. Membrane Science 377 (2011) 1-35.

755 [9] L. An, T.S. Zhao, L. Zeng, X.H. Yan, Performance of an alkaline direct ethanol
756 fuel cell with hydrogen peroxide as oxidant, Int. J. Hydrogen Energy 39 (2014)
757 2320-2324.

758 [10] L. Zeng, T.S. Zhao, L. An, A high-performance supportless silver nanowire
759 catalyst for anion exchange membrane fuel cells, J. Mater. Chem. A 3 (2015)
760 1410-1416.

761 [11] J. Cheng, G. He, F. Zhang, A mini-review on anion exchange membranes for fuel
762 cell applications: Stability issue and addressing strategies, Int. J. Hydrogen Energy 40
763 (2015) 7348-7360.

764 [12] S. Maurya, S.H. Shin, Y. Kim, S.H. Moon, A review on recent developments of
765 anion exchange membranes for fuel cells and redox flow batteries, RSC Adv. 5 (2015)
766 37206-37230.

767 [13] L. An, R. Chen, Mathematical modeling of direct formate fuel cells, Applied
768 Thermal Engineering 124 (2017) 232-240.

769 [14] M.A. Hickner, A.M. Herring, E.B. Coughlin, Anion exchange membranes:
770 Current status and moving forward, J. Polymer Science, Part B: Polymer Physics 51
771 (2013) 1727-1735.

772 [15] L. An, R. Chen, Recent progress in alkaline direct ethylene glycol fuel cells for
773 sustainable energy production, J. Power Sources 329 (2016) 484-501.

774 [16] L. An, T.S. Zhao, Transport phenomena in alkaline direct ethanol fuel cells for
775 sustainable energy production, J. Power Sources 341 (2017) 199-211.
776 [17] L. An, T.S. Zhao, L. Zeng, Agar chemical hydrogel electrode binder for
777 fuel-electrolyte-fed fuel cells, Applied Energy 109 (2013) 67-71.
778 [18] A.M. Bartrom, J.L. Haan, The direct formate fuel cell with an alkaline anion
779 exchange membrane, J. Power Sources 214 (2012) 68-74.
780 [19] L. An, T.S. Zhao, X.L. Zhou, L. Wei, X.H. Yan, A high-performance
781 ethanol-hydrogen peroxide fuel cell, RSC Advances 4 (2014) 65031-65034.
782 [20] J.R. Varcoe, R.C.T. Slade, Prospects for Alkaline Anion-Exchange Membranes in
783 Low Temperature Fuel Cells, Fuel Cells 5 (2005) 187-200.
784 [21] L. An, T.S. Zhao, X.L. Zhou, X.H. Yan, C.Y. Jung, A low-cost, high-performance
785 zinc–hydrogen peroxide fuel cell, J. Power Sources 275 (2015) 831-834.
786 [22] G. Couture, A. Alaaeddine, F. Boschet, B. Ameduri, Polymeric materials as
787 anion-exchange membranes for alkaline fuel cells. Progress in Polymer Science 36
788 (2011) 1521-1557.
789 [23] Z.F. Pan, R. Chen, L. An, Y.S. Li, Alkaline anion exchange membrane fuel cells
790 for cogeneration of electricity and valuable chemicals, J. Power Sources 365 (2017)
791 430-445.
792 [24] L. An, C.Y. Jung, Transport phenomena in direct borohydride fuel cells, Applied

793 Energy 205 (2017) 1270-1282.

794 [25] Z.J. Xia, S. Yuan, G.P. Jiang, X.X. Guo, J.H. Fang, L.L. Liu, J.L. Qiao, J. Yin,

795 Polybenzimidazoles with pendant quaternary ammonium groups as potential anion

796 exchange membranes for fuel cells, J. Membrane Science 390-391 (2012) 152-159.

797 [26] D. Henkensmeier, H. Cho, H. Kim, C.N. Kirchner, J. Leppin, A. Dyck, J.H. Jang,

798 E. Cho, S. Nam, T. Lim, Polybenzimidazolium hydroxides-Structure, stability and

799 degradation, Polymer Degradation and Stability 97 (2012) 264-272.

800 [27] H. Lee, J. Choi, J.Y. Han, H. Kim, Y. Sung, H. Kim, D. Henkensmeier, E.A. Cho,

801 J.H. Jang, S.J. Yoo, Synthesis and characterization of poly(benzimidazolium)

802 membranes for anion exchange membrane fuel cells, Polym. Bull. 70 (2013)

803 2619-2631.

804 [28] D. Henkensmeier, H. Cho, M. Brela, A. Michalak, A. Dyck, W. Germer, N.M.H.

805 Duong, J.H. Jang, H. Kim, N. Woo, T. Lim, Anion conducting polymers based on

806 ether linked polybenzimidazole (PBI-OO), Int. J. Hydrogen Energy 39 (2014)

807 2842-2853.

808 [29] L. Jheng, S.L. Hsu, B. Lin, Y. Hsu, Quaternized polybenzimidazoles with

809 imidazolium cation moieties for anion exchange membrane fuel cells, J. Membrane

810 Science 460 (2014) 160-170.

811 [30] A. Katzfuß, S. Poynton, J. Varcoe, V. Gogel, U. Storr, J. Kerres, Methylated

812 polybenzimidazole and its application as a blend component in covalently
813 cross-linked anion-exchange membranes for DMFC, J. Membrane Science 465 (2014)
814 129-137.
815 [31] J.S. Wainright, J.T. Wang, D. Weng, R.F. Savinell, M. Litt, Acid-doped
816 Polybenzimidazoles: A New Polymer Electrolyte, J. Electrochem. Soc. 142 (1995)
817 L121-L123.
818 [32] M. Okamoto, T. Fujigaya, N. Nakashima, Design of an Assembly of
819 Poly(benzimidazole), Carbon Nanotubes, and Pt Nanoparticles for a Fuel-Cell
820 Electrocatalyst with an Ideal Interfacial Nanostructure, Small 5 (2009) 735-740.
821 [33] M.R. Tarasevich, Z.R. Karichev, V.A. Bogdanovskaya, L.N. Kuznetsova, B.N.
822 Efremov, A.V. Kapustin, Electroconductance and penetrability of polybenzimidazole
823 membranes in alkaline solutions, Russ J Electrochem, 40 (2004) 653-656.
824 [34] R. He, Q. Li, A. Bach, J.O. Jensen, N.J. Bjerrum, Physicochemical properties of
825 phosphoric acid doped polybenzimidazole membranes for fuel cells, J. Membr. Sci.
826 277 (2006) 38-45.
827 [35] Q.X. Wu, H.Y. Li, W.X. Yuan, Z.K. Luo, F. Wang, H.Y. Sun, X.X. Zhao, H.D. Fu,
828 Performance evaluation of an air-breathing high-temperature proton exchange
829 membrane fuel cell, Applied Energy 160 (2015) 146-152.
830 [36] Q. Li, R. He, J.O. Jensen, N.J. Bjerrum. Approaches and Recent Development of

831 Polymer Electrolyte Membranes for Fuel Cells Operating above 100^{o}C. Chem. Mater.
832 15 (2003) 4896-4915.
833 [37] B. Xing, O. Savadogo, Hydrogen/oxygen polymer electrolyte membrane fuel
834 cells (PEMFCs) based on alkaline-doped polybenzimidazole (PBI), Electrochemistry
835 Communications 2 (2000) 697-702.
836 [38] H.Y. Hou, G.Q. Sun, R.H. He, B.Y. Sun, W. Jin, H. Liu, Q. Xin, Alkali doped
837 polybenzimidazole membrane for alkaline direct methanol fuel cell, Int. J. Hydrogen
838 Energy 33 (2008) 7172-7176.
839 [39] H.Y. Hou, G.Q. Sun, R.H. He, Z.M. Wu, B.Y. Sun, Alkali doped
840 polybenzimidazole membrane for high performance alkaline direct ethanol fuel cell, J.
841 Power Sources 182 (2008) 95-99.
842 [40] L. An, L. Zeng, T.S. Zhao, An alkaline direct ethylene glycol fuel cell with an
843 alkali-doped polybenzimidazole membrane, Int. J. Hydrogen Energy 38 (2013)
844 10602-10606.
845 [41] A.P. Nascimento, J.J. Linares, Performance of a Direct Glycerol Fuel Cell using
846 KOH Doped Polybenzimidazole as Electrolyte, J. Braz. Chem. Soc. 25 (2014)
847 509-516.
848 [42] J.H. Jiang, A. Wieckowski, Prospective direct formate fuel cell, Electrochemistry
849 Communications 18 (2012) 41-43.

850 [43] D.J. Chen, S.S. Yu, X. Liu, X.F. Li, Porous polybenzimidazole membranes with
851 excellent chemical stability and ion conductivity for direct borohydride fuel cells, J.
852 Power Sources 282 (2015) 323-327.
853 [44] O.E. Kongstein, T. Berning, B. Børresen, F. Seland, R. Tunold, Polymer
854 electrolyte fuel cells based on phosphoric acid doped polybenzimidazole (PBI)
855 membranes, Energy 32 (2007) 418-422.
856 [45] L. Zeng, T.S. Zhao, L. An, G. Zhao, X.H. Yan, Physicochemical properties of
857 alkaline doped polybenzimidazole membranes for anion exchange membrane fuel
858 cells, J. Membrane Science 493 (2015) 340-348.
859 [46] A.D. Modestov, M.R. Tarasevich, A. Y. Leykin, V.Y. Filimonov, MEA for
860 alkaline direct ethanol fuel cell with alkali doped PBI membrane and non-platinum
861 electrodes, J. Power Sources 188 (2009) 502-506.
862 [47] H.Y. Hou, S.L. Wang, Q. Jiang, W. Jin, L.H. Jiang, G.Q. Sun, Durability study of
863 KOH doped polybenzimidazole membrane for air-breathing alkaline direct ethanol
864 fuel cell, J. Power Sources 196 (2011) 3244-3248.
865 [48] H.Z. Luo, G. Vaivars, B. Agboola, S.C. Mu, M. Mathe, Anion exchange
866 membrane based on alkali doped poly(2,5-benzimidazole) for fuel cell, Solid State
867 Ionics 208 (2012) 52-55.
868 [49] D. Aili, M.K. Hansen, R.F. Renzaho, Q.F. Li, E. Christensen, J.O. Jensen, N.J.

869 Bjerrum, Heterogeneous anion conducting membranes based on linear and
870 crosslinked KOH doped polybenzimidazole for alkaline water electrolysis, J.
871 Membrane Science 447 (2013) 424-432.
872 [50] H. Zarrin, G.P. Jiang, G.Y.Y. Lam, M. Fowler, Z.W. Chen, High performance
873 porous polybenzimidazole membrane for alkaline fuel cells, Int. J. Hydrogen Energy
874 39 (2014) 18405-18415.
875 [51] J. Wu, C. Lo, L. Li, H. Li, C. Chang, K. Liao, C. Hu, Y. Liu, S.J. Lue, Thermally
876 stable polybenzimidazole/carbon nano-tube composites for alkaline direct methanol
877 fuel cell applications, J. Power Sources 246 (2014) 39-48.
878 [52] L. An, T.S. Zhao, Q.X. Wu, L. Zeng, Comparison of different types of membrane
879 in alkaline direct ethanol fuel cells, Int. J. Hydrogen Energy 37 (2012) 14536-14542.
880 [53] M. Han, G. Zhang, Z. Liu, S. Wang, M. Li, J. Zhu, H. Li, Y. Zhang, C.M. Lew, H.
881 Na, Cross-linked polybenzimidazole with enhanced stability for high temperature
882 proton exchange membrane fuel cells, J. Mater. Chem. 21 (2011) 2187-2193.
883 [54] L. Zeng, T.S. Zhao, L. An, G. Zhao, X.H. Yan, A high-performance
884 sandwiched-porous polybenzimidazole membrane with enhanced alkaline retention
885 for anion exchange membrane fuel cells, Energy Environ. Sci. 8 (2015) 2768-2774.
886 [55] S. Xu, G. Zhang, Y. Zhang, C. Zhao, L. Zhang, M. Li, J. Wang, N. Zhang, H. Na,
887 Cross-linked hydroxide conductive membranes with side chains for direct methanol

fuel cell applications, J. Materials Chemistry 22 (2012) 13295-13302.

[56] A.Y. Leykin, O.A. Shkrebko, M.R. Tarasevich, Ethanol crossover through alkali-doped polybenzimidazole membrane, J. Membrane Science 328 (2009) 86-89.

[57] L. An, T.S. Zhao, Y.S. Li, Q.X. Wu, Charge carriers in alkaline direct oxidation fuel cells, Energy Environ. Sci. 5 (2012) 7536-7538.

[58] K. Matsumoto, T. Fujigaya, H. Yanagi, N. Nakashima, Very High Performance Alkali Anion-Exchange Membrane Fuel Cells, Adv. Funct. Mater. 21 (2011) 1089-1094.

[59] X.L. Zhou, T.S. Zhao, L. An, L. Wei, C. Zhang, The use of polybenzimidazole membranes in vanadium redox flow batteries leading to increased coulombic efficiency and cycling performance, Electrochim. Acta 153 (2015) 492-498.

[60] L.Y. Li, B.C. Yu, C.M. Shih, S.J. Lue, Polybenzimidazole membranes for direct methanol fuel cell: Acid-doped or alkali-doped?, J. Power Sources 287 (2015) 386-395.

[61] R.N. Couto, J.J. Linares, KOH-doped polybenzimidazole for alkaline direct glycerol fuel cells, J. Membrane Science 486 (2015) 239-247.

907

908 **Table caption:**

909 Table 1 The selected fuel cell performance achieved by using alkali-doped

910 polybenzimidazole membranes.

911 **Figure captions:**

912 Fig. 1 Chemical structure of the pristine polybenzimidazole membrane [59].

913 Reproduced with permission from Elsevier.

914 Fig. 2 (a) The scheme of combination between KOH and -NH- [39]. (b) The possible

915 combination mechanism in details [47]. (c) The possible reaction during the doping

916 process: neutralization reaction and the hydrogen bonds before and after the doping

917 process [45]. (d) Schematic of the pristine PBI membrane and alkali-doped PBI

918 membrane [45]. Reproduced with permission from Elsevier.

919 Fig. 3 (a) Experimental setup and flow chart [57]. (b) Variations in the Na^+ flux

920 through each of three membranes with current density [57]. Reproduced with

921 permission from The Royal Society of Chemistry.

922 Fig. 4 (a) Effect of the doping time on the doping level [48]. (b) The ionic

923 conductivity as a function of the time. [47]. (c) Effect of the NaOH concentration on

924 the ionic conductivity [52]. (d) Variation of the ionic conductivity with the doping

925 electrolyte cocnentration at vairous K_2CO_3 concentrations [37]. Reproduced with

926 permission from Elsevier.

927 Fig. 5 (a) Effect of the temperature on the ionic conductivity [52]. (b) Variation of the
928 conductivity of the KOH-doped PBI memrbane with the temperature [37]. (c) Effect
929 of the soaking time on the ionic conductivity [52]. (d) Ion conductivities of the
930 alkali-doped PBI membrane in 1.0 M NaOH [48]. Reproduced with permission from
931 Elsevier.

932 Fig. 6 (a) The fabrication process of KOH-doped porous PBI membranes [50]. (b) The
933 polarization and power density curves using three membranes [50]. (c) Schematic
934 illustration of a PBI-based membrane electrode assembly and the fuel cell [54]. (d)
935 The polarization and power density curves with the conventional MEA (round
936 symbols) and the novel MEA (square symbols), and the constant current discharging
937 behaviors using the conventional MEA and the novel MEA at a current density of 700
938 mA cm^{-2} [54]. Reproduced with permission from Elsevier and The Royal Society of
939 Chemistry.

940 Fig. 7 (a) Schematic illustration of an anion exchange membrane fuel cell [58]. (b)
941 The polarization and power density curves of the fuel cell (red line: PyPBI cell; black
942 line: AS-4 cell) [58]. (c) The polarization curves of an alkaline direct ethanol fuel cell
943 with alkali-doped PBI membrane at 75^{o}C and 90^{o}C [38]. (d) The performance of
944 direct methanol fuel cells using a KOH-doped PBI membrane and H_3PO_4-doped PBI

membrane at 60°C (upper) and 90°C (lower), respectively [60]. (e) The performance of an air-breathing alkaline direct ethanol fuel cell at 60°C [47]. Reproduced with permission from Wiley and Elsevier.

Fig. 8 (a) Temperatuere dependence of polarization curves for a direct formate fuel cell with a fuel of 2.0 M KOH + 2.0 M HCOOK [42]. (b) HCOOK cocnentration dependence of polarization and power density curves for a direct formate fuel cell at 120°C [42]. (c) Schematic of the designed membrane [43]. (d) The polarization and power density curves of direct borohydride fuel cells with the prepared membranes [43]. Reproduced with permission from Elsevier.

Graphical Abstract:

This article provides a review of past research on the alkali-doped polybenzimidazole membranes and their application in fuel cells, as well as the fuel cell performance.

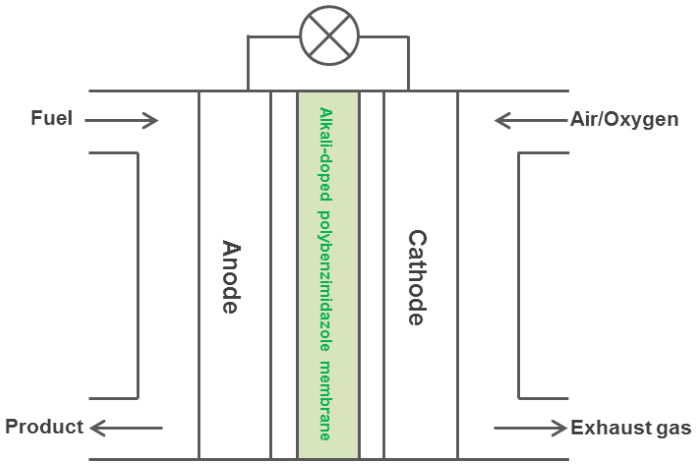

959

960

961 **Highlights**

962 • This article reviews the past research on alkali-doped PBI membranes.

963 • Particular attention is paid to their physicochemical properties.

964 • Selected single-cell performance is summarized and discussed.

965

966

Fuel/Oxidant	Anode	Cathode	Membrane	T (°C)	Power density (mW cm^{-2})	Ref.
1200 sccm H_2 / 800 sccm O_2	Pt/C (0.35 mg cm^{-2})	Pt/C (0.35 mg cm^{-2})	KOH-doped PBI membrane	50	~700 @ 2.0 A cm^{-2}	[37]
1200 sccm H_2 / 800 sccm O_2	Pt/C (0.35 mg cm^{-2})	Pt/C (0.35 mg cm^{-2})	(KOH + K_2CO_3)-doped PBI membrane	50	~700 @ 2.0 A cm^{-2}	[37]
1000 sccm H_2 (RH = 95%) / 2000 sccm air (RH = 95%)	Pt/C (0.45 mg cm^{-2}) (MWNT/KOH-PyPBI)	Pt/C (0.45 mg cm^{-2}) (MWNT/KOH-PyPBI)	Tokuyama A2012 membrane	50	256	[58]

1000 sccm H_2 (RH = 95%) / 2000 sccm air (RH = 95%)	Pt/C (0.45 mg cm^{-2}) (Tokuyama AS-4)	Pt/C (0.45 mg cm^{-2}) (Tokuyama AS-4)	Tokuyama A2012 membrane	50	174	[58]
200 sccm H_2 (RH = 100%) / 200 sccm O_2 (RH = 100%)	Pt/C (0.5 mg cm^{-2})	Pt/C (0.5 mg cm^{-2})	KOH-doped porous PBI membrane	60	72.17	[50]
200 sccm H_2 (RH = 100%) / 200 sccm O_2 (RH = 100%)	Pt/C (0.5 mg cm^{-2})	Pt/C (0.5 mg cm^{-2})	Fumapem® FAA membrane	60	45.36	[50]
200 sccm H_2 (RH = 100%) / 200 sccm O_2 (RH = 100%)	Pt/C (0.5 mg cm^{-2})	Pt/C (0.5 mg cm^{-2})	KOH-doped PBI membrane	60	41.26	[50]
300 sccm H_2 (RH = 100%) / 300 sccm O_2 (RH = 100%)	Pd NWs /PBI/rGO	Pd NWs /PBI/rGO	KOH-doped sandwiched-porous PBI membrane	90	544.4	[54]
300 sccm H_2 (RH = 100%) / 300 sccm O_2 (RH = 100%)	Pd NWs /PBI/rGO	Pd NWs /PBI/rGO	KOH-doped PBI membrane	90	396.8	[54]
5 mL min^{-1} 1 M methanol + 6 M KOH / 100 sccm O_2 (RH = 100%)	PtRu/C (5 mg cm^{-2})	Pt/C (5 mg cm^{-2})	KOH-doped PBI/0.05% CNT composite membrane	60	49.9	[51]
5 mL min^{-1} 2 M methanol + 6 M KOH / 100 sccm O_2 (RH = 100%)	PtRu/C (5 mg cm^{-2})	Pt/C (5 mg cm^{-2})	KOH-doped PBI/0.05% CNT composite membrane	60	67.1	[51]
5 mL min^{-1} 1 M methanol + 6 M KOH / 100 sccm humidified O_2	PtRu (5 mg cm^{-2})	Pt (5 mg cm^{-2})	KOH-doped PBI membrane	60	66.5	[60]
5 mL min^{-1} 2 M	PtRu	Pt	KOH-doped PBI	60	81.5	[60]

methanol + 6 M KOH / 100 sccm humidified O_2	(5 mg cm^{-2})	(5 mg cm^{-2})	membrane			
15 mL min^{-1} 1 M methanol + 6 M KOH / 100 sccm humidified O_2	PtRu (5 mg cm^{-2})	Pt (5 mg cm^{-2})	KOH-doped PBI membrane	60	120	[60]
1 mL min^{-1} 2 M methanol + 2 M KOH / O_2	PtRu/C (2.0 mg cm^{-2})	Pt/C (1.0 mg cm^{-2})	KOH-doped PBI membrane	90	31	[38]
5 mL min^{-1} 1 M methanol + 6 M KOH / 100 sccm O_2 (RH = 100%)	PtRu/C (5 mg cm^{-2})	Pt/C (5 mg cm^{-2})	KOH-doped PBI membrane	90	24.5	[51]
5 mL min^{-1} 1 M methanol + 6 M KOH / 100 sccm O_2 (RH = 100%)	PtRu/C (5 mg cm^{-2})	Pt/C (5 mg cm^{-2})	KOH-doped PBI/0.05% CNT composite membrane	90	50.9	[51]
5 mL min^{-1} 2 M methanol + 6 M KOH / 100 sccm O_2 (RH = 100%)	PtRu/C (5 mg cm^{-2})	Pt/C (5 mg cm^{-2})	KOH-doped PBI/0.05% CNT composite membrane	90	104.7	[51]
5 mL min^{-1} 2 M methanol + 6 M KOH / 100 sccm O_2 (RH = 100%)	PtRu/C (5 mg cm^{-2})	Pt/C (5 mg cm^{-2})	KOH-doped PBI/0.10% CNT composite membrane	90	~100	[51]
5 mL min^{-1} 2 M methanol + 6 M KOH / 100 sccm O_2 (RH = 100%)	PtRu/C (5 mg cm^{-2})	Pt/C (5 mg cm^{-2})	KOH-doped PBI/0.15% CNT composite membrane	90	~40	[51]
5 mL min^{-1} 2 M methanol + 6 M KOH / 100 sccm O_2 (RH = 100%)	PtRu/C (5 mg cm^{-2})	Pt/C (5 mg cm^{-2})	KOH-doped PBI/1% CNT composite membrane	90	~60	[51]
5 mL min^{-1} 1 M methanol + 6 M KOH / 100 sccm humidified O_2	PtRu (5 mg cm^{-2})	Pt (5 mg cm^{-2})	KOH-doped PBI membrane	90	109.3	[60]

5 mL min^{-1} 2 M methanol + 6 M KOH / 100 sccm humidified O_2	PtRu (5 mg cm^{-2})	Pt (5 mg cm^{-2})	KOH-doped PBI membrane	90	117.9	[60]
15 mL min^{-1} 1 M methanol + 6 M KOH / 100 sccm humidified O_2	PtRu (5 mg cm^{-2})	Pt (5 mg cm^{-2})	KOH-doped PBI membrane	90	158.9	[60]
1 mL min^{-1} 2 M ethanol + 2 M KOH / air	PtRu/C (2 mg cm^{-2})	MnO_2/C (1 mg cm^{-2})	KOH-doped PBI membrane	60	30 (0 h)	[47]
1 mL min^{-1} 2 M ethanol + 2 M KOH / air	PtRu/C (2 mg cm^{-2})	MnO_2/C (1 mg cm^{-2})	KOH-doped PBI membrane	60	15 (210 h)	[47]
1 mL min^{-1} 2 M ethanol + 2 M KOH / air	PtRu/C (2 mg cm^{-2})	MnO_2/C (1 mg cm^{-2})	KOH-doped PBI membrane	60	14 (220 h)	[47]
1 mL min^{-1} 2 M ethanol + 2 M KOH / air	PtRu/C (2 mg cm^{-2})	MnO_2/C (1 mg cm^{-2})	KOH-doped PBI membrane	60	9 (240 h)	[47]
1 mL min^{-1} 2 M ethanol + 2 M KOH / O_2	PtRu/C (2 mg cm^{-2})	Pt/C (1 mg cm^{-2})	KOH-doped PBI membrane	75	49.20	[39]
5 mL min^{-1} 2 M ethanol + 3 M KOH / 200 sccm air	RuV/C (2.1 mg cm^{-2})	Pt/C (1.24 mg cm^{-2})	KOH-doped PBI membrane	80	90	[46]
5 mL min^{-1} 2 M ethanol + 3 M KOH / 200 sccm O_2	RuV/C (2.1 mg cm^{-2})	Pt/C (1.24 mg cm^{-2})	KOH-doped PBI membrane	80	110	[46]
5 mL min^{-1} 2 M ethanol + 3 M KOH / 200 sccm air	RuV/C (4.5 mg cm^{-2})	TMPhP/C (9.2 mg cm^{-2})	KOH-doped PBI membrane	80	~105	[46]
5 mL min^{-1} 2 M ethanol + 3 M KOH / 200 sccm	RuV/C (4.5 mg cm^{-2})	TMPhP/C (9.2 mg cm^{-2})	KOH-doped PBI membrane	80	~120	[46]

O_2						
5 mL min^{-1} 2 M ethanol + 3 M KOH / 200 sccm air	RuV/C (0.72 mg cm^{-2})	TMPhP/C (9 mg cm^{-2})	KOH-doped PBI membrane	80	35	[46]
1 mL min^{-1} 2 M ethanol + 2 M KOH / O_2	PtRu/C (2 mg cm^{-2})	Pt/C (1 mg cm^{-2})	KOH-doped PBI membrane	90	60.95	[39]
2 mL min^{-1} 0.5 M EG +1 M KOH / 100 sccm O_2	PdNi/C (1 mg cm^{-2})	HYPERMEC™/C (1 mg cm^{-2})	KOH-doped PBI membrane	60	28	[40]
2 mL min^{-1} 1 M EG +1 M KOH / 100 sccm O_2	PdNi/C (1 mg cm^{-2})	HYPERMEC™/C (1 mg cm^{-2})	KOH-doped PBI membrane	60	32	[40]
2 mL min^{-1} 2 M EG +1 M KOH / 100 sccm O_2	PdNi/C (1 mg cm^{-2})	HYPERMEC™/C (1 mg cm^{-2})	KOH-doped PBI membrane	60	23	[40]
2 mL min^{-1} 1 M EG +3 M KOH / 100 sccm O_2	PdNi/C (1 mg cm^{-2})	HYPERMEC™/C (1 mg cm^{-2})	KOH-doped PBI membrane	60	58	[40]
2 mL min^{-1} 1 M EG +5 M KOH / 100 sccm O_2	PdNi/C (1 mg cm^{-2})	HYPERMEC™/C (1 mg cm^{-2})	KOH-doped PBI membrane	60	72	[40]
2 mL min^{-1} 1 M EG +7 M KOH / 100 sccm O_2	PdNi/C (1 mg cm^{-2})	HYPERMEC™/C (1 mg cm^{-2})	KOH-doped PBI membrane	60	80	[40]
2 mL min^{-1} 1 M EG +9 M KOH / 100 sccm O_2	PdNi/C (1 mg cm^{-2})	HYPERMEC™/C (1 mg cm^{-2})	KOH-doped PBI membrane	60	38	[40]
2 mL min^{-1} 1 M EG +7 M KOH / 100 sccm O_2	PdNi/C (1 mg cm^{-2})	HYPERMEC™/C (1 mg cm^{-2})	KOH-doped PBI membrane	90	112	[40]
2 mL min^{-1} 1 M EG +7 M KOH / 100 sccm Air	PdNi/C (1 mg cm^{-2})	HYPERMEC™/C (1 mg cm^{-2})	KOH-doped PBI membrane	90	92	[40]
1 mL min^{-1} 1 M glycerol + 4 M KOH / 20 sccm	Pt/C (2 mg cm^{-2})	Pt/C (1 mg cm^{-2})	KOH-doped PBI membrane	30	~5	[41]

O_2						
1 mL min^{-1} 1 M glycerol + 4 M KOH / 20 sccm O_2	Pt_3Sn/C (2 mg cm^{-2})	Pt/C (1 mg cm^{-2})	KOH-doped PBI membrane	30	~8	[61]
1 mL min^{-1} 1 M glycerol + 4 M KOH / 20 sccm O_2	Pt/C (2 mg cm^{-2})	Pt/C (1 mg cm^{-2})	KOH-doped PBI membrane	45	~8	[41]
1 mL min^{-1} 1 M glycerol + 4 M KOH / 20 sccm O_2	Pt_3Sn/C (2 mg cm^{-2})	Pt/C (1 mg cm^{-2})	KOH-doped PBI membrane	45	~17	[61]
1 mL min^{-1} 1 M glycerol + 4 M KOH / 20 sccm O_2	Pt/C (2 mg cm^{-2})	Pt/C (1 mg cm^{-2})	KOH-doped PBI membrane	60	~12	[41]
1 mL min^{-1} 0.5 M glycerol + 4 M KOH / 20 sccm O_2	Pt/C (2 mg cm^{-2})	Pt/C (1 mg cm^{-2})	KOH-doped PBI membrane	60	~16	[41]
1 mL min^{-1} 2 M glycerol + 4 M KOH / 20 sccm O_2	Pt/C (2 mg cm^{-2})	Pt/C (1 mg cm^{-2})	KOH-doped PBI membrane	60	~14	[41]
1 mL min^{-1} 4 M glycerol + 4 M KOH / 20 sccm O_2	Pt/C (2 mg cm^{-2})	Pt/C (1 mg cm^{-2})	KOH-doped PBI membrane	60	~7	[41]
1 mL min^{-1} 1 M glycerol + 2 M KOH / 20 sccm O_2	Pt/C (2 mg cm^{-2})	Pt/C (1 mg cm^{-2})	KOH-doped PBI membrane	60	~6	[41]
1 mL min^{-1} 1 M glycerol + 3 M KOH / 20 sccm O_2	Pt/C (2 mg cm^{-2})	Pt/C (1 mg cm^{-2})	KOH-doped PBI membrane	60	~9	[41]
1 mL min^{-1} 1 M	Pt/C	Pt/C	KOH-doped PBI	60	~18	[41]

glycerol + 6 M KOH / 20 sccm O_2	(2 mg cm^{-2})	(1 mg cm^{-2})	membrane			
0.5 mL min^{-1} 1 M glycerol + 4 M KOH / 20 sccm O_2	Pt/C (2 mg cm^{-2})	Pt/C (1 mg cm^{-2})	KOH-doped PBI membrane	60	~11	[41]
2 mL min^{-1} 1 M glycerol + 4 M KOH / 20 sccm O_2	Pt/C (2 mg cm^{-2})	Pt/C (1 mg cm^{-2})	KOH-doped PBI membrane	60	~14	[41]
4 mL min^{-1} 1 M glycerol + 4 M KOH / 20 sccm O_2	Pt/C (2 mg cm^{-2})	Pt/C (1 mg cm^{-2})	KOH-doped PBI membrane	60	~14	[41]
1 mL min^{-1} 1 M glycerol + 4 M KOH / 20 sccm O_2	Pt_3Sn/C (2 mg cm^{-2})	Pt/C (1 mg cm^{-2})	KOH-doped PBI membrane	60	~22	[61]
1 mL min^{-1} 1 M glycerol + 4 M KOH / 20 sccm O_2	Pt/C (2 mg cm^{-2})	Pt/C (1 mg cm^{-2})	KOH-doped PBI membrane	75	18	[41]
1 mL min^{-1} 1 M glycerol + 4 M KOH / 20 sccm O_2	Pt_3Sn/C (2 mg cm^{-2})	Pt/C (1 mg cm^{-2})	KOH-doped PBI membrane	75	34.2	[61]
1 mL min^{-1} 1 M glycerol + 4 M KOH / 20 sccm O_2	Pt/C (2 mg cm^{-2})	Pt/C (1 mg cm^{-2})	KOH-doped PBI membrane	90	15	[41]
2 mL min^{-1} 1 M glycerol + 4 M KOH / 20 sccm O_2	Pt_3Sn/C (2 mg cm^{-2})	Pt/C (1 mg cm^{-2})	KOH-doped PBI membrane	60	~17	[41]
2 mL min^{-1} 1 M glycerol + 4 M KOH / 20 sccm	PtRu/C (2 mg cm^{-2})	Pt/C (1 mg cm^{-2})	KOH-doped PBI membrane	60	~15	[41]

O_2						
6 mL min^{-1} 2 M HCOOK + 2 M KOH / 200 sccm O_2	Pd/C (4 mg cm^{-2})	Ag/C (8 mg cm^{-2})	KOH-doped PBI membrane (FuMA-Tech GmBH)	120	170	[29]
6 mL min^{-1} 6 M HCOOK + 2 M KOH / 200 sccm O_2	Pd/C (4 mg cm^{-2})	Ag/C (8 mg cm^{-2})	KOH-doped PBI membrane (FuMA-Tech GmBH)	120	160	[29]
0.5 mL min^{-1} 1 M $NaBH_4$ + 3 M NaOH / O_2	Pt/C (1 mg cm^{-2})	Pt/C (0.5 mg cm^{-2})	NaOH-doped porous PBI membrane (0.45)	40	204	[43]
0.5 mL min^{-1} 1 M $NaBH_4$ + 3 M NaOH / O_2	Pt/C (1 mg cm^{-2})	Pt/C (0.5 mg cm^{-2})	NaOH-doped porous PBI membrane (0.6)	40	262	[43]
0.5 mL min^{-1} 1 M $NaBH_4$ + 3 M NaOH / O_2	Pt/C (1 mg cm^{-2})	Pt/C (0.5 mg cm^{-2})	NaOH-doped porous PBI membrane (0.8)	40	151	[43]

Table 1 The selected fuel cell performance achieved by using alkali-doped polybenzimidazole membranes.